Structural and Functional Imaging

CHAPTER 4

Dr. Conor Waters[1], Dr. Nathan Hearn[1], Dr. Cassandra Williams[1], Dr. Shisheng Lu[1], Dr. Jeffrey Lai[1],A/Prof. Frank Gaillard[1]

[1] *Royal Melbourne Hospital, Melbourne, Australia*

Introduction

The role of imaging in neuropsychiatry is different to many other areas of neuroradiology. In many cases, the imaging findings are non-specific, and it is rare for a diagnosis to be made based on imaging alone. The role of the radiologist is to collaborate with physicians in coming to the most reasonable diagnosis or set of differential diagnoses, through consideration of pre-test probability given patient presentation, and determining whether imaging findings support or oppose this assessment. Given the collaborative nature of these cases, the clinical information provided in imaging requests and provided at multidisciplinary meetings is crucial for the radiologist, and at minimum should include demographics, symptoms, relevant negatives, working diagnosis and differential diagnoses. Notably, structural atrophy is a late and often non-specific finding in the course of many neuropsychiatric conditions (e.g. Alzheimer's Disease), and imaging at several time points may be required to establish the diagnosis.

In this chapter, we will firstly outline the general approach to radiological assessment in neuropsychiatry, discussing the role of structural and functional imaging. We will then discuss individual neuropsychiatric conditions where imaging, both structural and functional, play important roles in diagnosis.

Imaging Modalities

There are roles for computed tomography (CT), magnetic resonance imaging (MRI) and nuclear medicine in neuropsychiatry.

- CT is often the first scan to be performed as it is the most accessible and can rule out other pathologies such as intracranial haemorrhage or space-occupying lesions[1]. It is more easily performed than MRI or positron emission tomography (PET) in patients with severe cognitive impairment, movement disorders, or agitation, and the spatial resolution and multiplanar reconstruction capacity of modern CT scanners allows for atrophy assessment to an extent.
- MRI is the mainstay of neuropsychiatric structural imaging. It provides excellent soft tissue contrast and spatial resolution, and can provide advanced characterisation of tissue characteristics such as diffusibility[2]. Imaging can be performed at both 1.5T and 3T field strengths, although subtle findings may be better appreciated on the latter.
- Nuclear medicine studies such as single-photon emission computed tomography (SPECT) and positron emission tomography (PET) complement the structural assessment of CT and MRI by providing functional information, such as perfusion or metabolism, which predate gross atrophy and can assist in early diagnosis and intervention[1]. Novel radiotracers have been developed for specific pathological correlates of neurodegenerative conditions, such as amyloid- and tau-targeted compounds; however, access to many of these compounds is limited outside of larger centres in developed countries[3].

MRI Protocol

Table 1 gives an overview of the common MRI sequences used in neuropsychiatry. The standard protocol for MRI in neuropsychiatry includes T1-weighted, T2-weighted, fluid attenuated inversion recovery (FLAIR), susceptibility-weighted imaging (SWI) and diffuse-weighted imaging (DWI) sequences.

T1-weighted

Three-dimensional (3D) isotropic acquisition of the T1-weighted sequence is preferred over the traditional two-dimensional sequence as it allows multiplanar reformats, including oblique coronal views through the hippocampi, which is helpful in assessing hippocampal volume. In addition, the 3D gradient-echo based T1-weighted sequences allows for automated morphometry, which is increasingly utilized to quantitatively assess regional brain volume[4]. Morphometry segments the brain into sections and calculates volume relative to the normal range for the patient's age and gender, displaying the data as a colour map according to z-score (see Figure 2 as example).

T2-weighted and FLAIR

The T2-weighted and FLAIR sequences are often referred to as the "pathology sequence" due to their sensitivity to tissue water content (Mnemonic: **T2** loves **W**ater, because water is H_20 i.e. water is bright on T2) . The FLAIR sequence has the added advantage of being more sensitive in detecting periventricular lesions by nulling the signal of the cerebrospinal fluid (CSF) in the ventricles[5].

SWI

SWI sequence is sensitive to substances that distort local magnetic fields such as degradation products of haemoglobin, iron and calcification[6]. The phase filtered map may help distinguish diamagnetic substances (e.g. calcification) from paramagnetic substances (e.g. haemosiderin) as both substances will cause signal loss on the SWI sequence. CT is also particularly useful in differentiating haemorrhage and calcification.

DWI

DWI sequence measures the diffusivity of water molecules within the tissue[7]. Tissues with restricted diffusion will be bright on the trace diffusion-weighted image and dark on the apparent diffusion coefficient (ADC) map. While it is most commonly used to detect acute infarcts, there are many other pathologies that can cause restricted diffusion and it has a key role in the imaging diagnosis of Creutzfeldt-Jakob disease.

Table 1; An overview of the MRI sequences used in neuropsychiatry and their main applications.

Sequence	Structures and Pathology Assessed
Sagittal T1	Anatomical overview Regional volume loss. Corpus callosum development and size. Brainstem and cerebellar volume. Hippocampal volume.
Coronal T1	Hippocampal volume. *Used to calculate mesial temporal lobe atrophy score (MTA) and Entorhinal Cortex Atrophy Score (ERICA) in Alzheimer's.*

Sequence	Structures and Pathology Assessed
Axial T1 + Morphometry	Anatomical overview. Regional volume loss. Morphometry maps display volume as a colour map relative to normal values of normal controls. Volume and signal of the basal ganglia.
Axial FLAIR	Highlights variation in signal of the brain parenchyma based on water content. *Used to assess for gliosis, chronic microvascular ischaemia, tumours, oedema and demyelination*
Axial T2	Arterial flow voids *Used to assess for arterial stenoses or occlusions and identifying aneurysms.* Similar to FLAIR, it can identify variation in signal of the brain parenchyma based on water content, although assessment is more difficult without CSF signal suppression.
Diffusion-weighted imaging (DWI) and ADC map	Assesses the diffusivity of tissue *Used to diagnose infarcts and the findings in Creutzfeldt-Jakob disease are best appreciated on DWI.*
Susceptibility-weighted imaging (SWI)	Identifies substances that distort the magnetic field *Used to identify microhaemorrhages, superficial siderosis and calcification.* The phase filtered map helps distinguish between diamagnetic (calcification) and paramagnetic (haemorrhage) substances.

Nuclear Medicine

While SPECT has historically been an important modality in neuropsychiatric and dementia imaging, and continues to be used in some centres, the current mainstay of nuclear medicine imaging in the investigation of neuropsychiatric disorders is PET. Co-registration of SPECT or PET to a concurrent CT provides improved image quality, localisation and quantification of metabolic findings. Nuclear medicine imaging software packages may also provide statistical mapping, which can provide a quantitative comparison of radiotracer activity compared to a normal age-matched population. Table 2 provides a summary of SPECT and PET radiotracers. A selection of more commonly used tracers are discussed below.

Glucose analogue tracers Fluorodeoxyglucose is the workhorse of neuropsychiatric PET imaging, most commonly used in workup of dementia presentations. As a glucose analogue, FDG provides visualisation of the altered neuronal activity and hypometabolism that occur early in a range of neurodegenerative conditions[8]. Distinctive patterns of cortical hypometabolism can be seen in many neurodegenerative conditions - for example, Alzheimer's disease classically involves hypometabolism of the posterior cingulate gyrus, precuneus, and temporoparietal lobes. *Amyloid tracers* Specific radiotracers with high affinity for fibrillar amyloid aggregates have made amyloid PET imaging an adjunct to FDG PET in the investigation of Alzheimer's disease and other b-amyloid deposition diseases. While the presence of amyloid plaques is not diagnostic of Alzheimer's disease, detection can support or refute the diagnosis in cases where clinical history and/or FDG PET findings are indeterminate[9]. Amyloid PET is also playing an increasing role in determining eligibility for anti-b-amyloid therapeutics, as well as in monitoring treatment response[10]. *Tau tracers*

Recently, tau tracers have been developed with high affinity for the neurofibrillary tangles that accumulate in AD and other tauopathies, such as progressive supranuclear palsy, and corticobasal degeneration[11]. Tau tracers have shown greater specificity in distinguishing AD from non-AD pathologies, however amyloid tracers remain more sensitive in the early diagnosis of AD and in guiding anti-amyloid therapy treatment.

Dopaminergic pathway tracers

This subset of radiotracers target dopaminergic pathways in the brain, and are used to detect presynaptic dopaminergic deficits in Parkinsonian syndromes (Parkinson's disease, multisystem atrophy, corticobasal degeneration, and progressive supranuclear palsy)[12]. They are useful in differentiating between neurodegenerative and non-neurodegenerative causes of parkinsonism, and in many cases also aids in differentiation of Alzheimer's disease from dementia with Lewy bodies. Currently, PET is less readily available than dopamine transporter (DAT) SPECT imaging in assessing presynaptic dopaminergic integrity.

Table 2: An overview of the Nuclear Medicine studies used in neuropsychiatry and their main applications.

Modality & Tracer group	Radiotracer	Pathology assessed
Positron emission tomography (PET)		
Glucose analogue	^{18}F FDG*	Alzheimer's disease (and variants) Frontotemporal lobar degeneration Vascular dementia Dementia with Lewy bodies Parkinsonian syndromes o Parkinson's disease o Supranuclear palsy o Multiple system atrophy Huntington disease
Amyloid	^{18}F Florbetaben ^{18}F Florbetapir ^{18}F Flutemetamol	Alzheimer's disease
Tau	^{18}F Flortaucipir	Alzheimer's disease
Dopaminergic pathway	^{18}F FDOPA** ^{18}F-AV-133 VMAT2***	Parkinsonian syndromes Dementia with Lewy bodies
Single-photon emission computed tomography (SPECT)		
	^{123}I Ioflupane (DaTscan^{D})	Parkinsonian syndromes Dementia with Lewy bodies

Modality & Tracer group	Radiotracer	Pathology assessed
	^{99m}Tc HMPAO^{+} ^{99m}Tc ECD^{++}	Alzheimer's disease Frontotemporal lobar degeneration Vascular dementia
	^{111}In DTPA^{+++} ^{99m}Tc DTPA	Normal pressure hydrocephalus

*fluorine-18 fluorodeoxyglucose, **fluorine-18 fluoro-dihydroxyphenylalanine, ***fluorine-18-9-fluoropropyl-(+)-dihydrotetrabenazine (AV-133) vesicular monoamine transporter type 2, ^{D}dopamine transporter scan, +technetium-99m hexamethylpropyleneamine oxime, ++technetium-99m ethyl cysteinate dimer, +++indium-111 diethylene triaminepentaacetic acid, ^currently under investigation

Dementia Disorders

Alzheimer disease

Key structural findings (MRI)	Atrophy in the mesial temporal lobe (hippocampus and entorhinal cortex) and posterior cingulate gyrus [1]
Supportive findings	May co-exist with cerebral amyloid angiopathy
Nuclear medicine	FDG PET: ↓ parietotemporal cortex (notably the precuneus), posterior cingulate cortex Additionally, variants may demonstrate: • Posterior cortical atrophy (PCA): ↓ occipital cortex, posterior temporal cortex • Logopaenic variant primary progressive aphasia (lvPPA): ↓ lateral temporal cortex, inferior parietal lobule, changes left >> right • Behavioural variant Alzheimer disease (bvAD): ↓ frontal and anterior temporal cortices Amyloid PET: ↑ diffuse cortical uptake Tau PET: mesial temporal lobe (early involvement), lateral temporal cortex, posterior cingulate cortex, parietal cortex [13]
Variants	PCA: Predominant parieto-occipital involvement [14] lvPPA: Predominant left posterior temporal and parietal lobe involvement Early onset: Temporoparietal and subcortical grey matter involvement
Radiological grading	Mesial temporal atrophy score (MTA) Entorhinal cortical atrophy score (ERICA) Posterior cortical atrophy score (Koedam) Boston criteria 2.0 (cerebral amyloid angiopathy)

The characteristic structural imaging finding in Alzheimer disease is atrophy of the mesial temporal lobe structures, typically but not always symmetrical, in a patient over 75 years of age presenting with cognitive impairment. This is often accompanied by atrophy of the posterior cingulate, parietal

and temporal cortices. The morphological features of atrophy develop late in the course of the disease and are usually present by the time clinical symptoms become apparent[15]. Posterior cingulate and parietotemporal hypometabolism on FDG PET can help differentiate early AD from other dementias[8]. Amyloid PET is likely to play an increasing role in AD diagnosis and management with

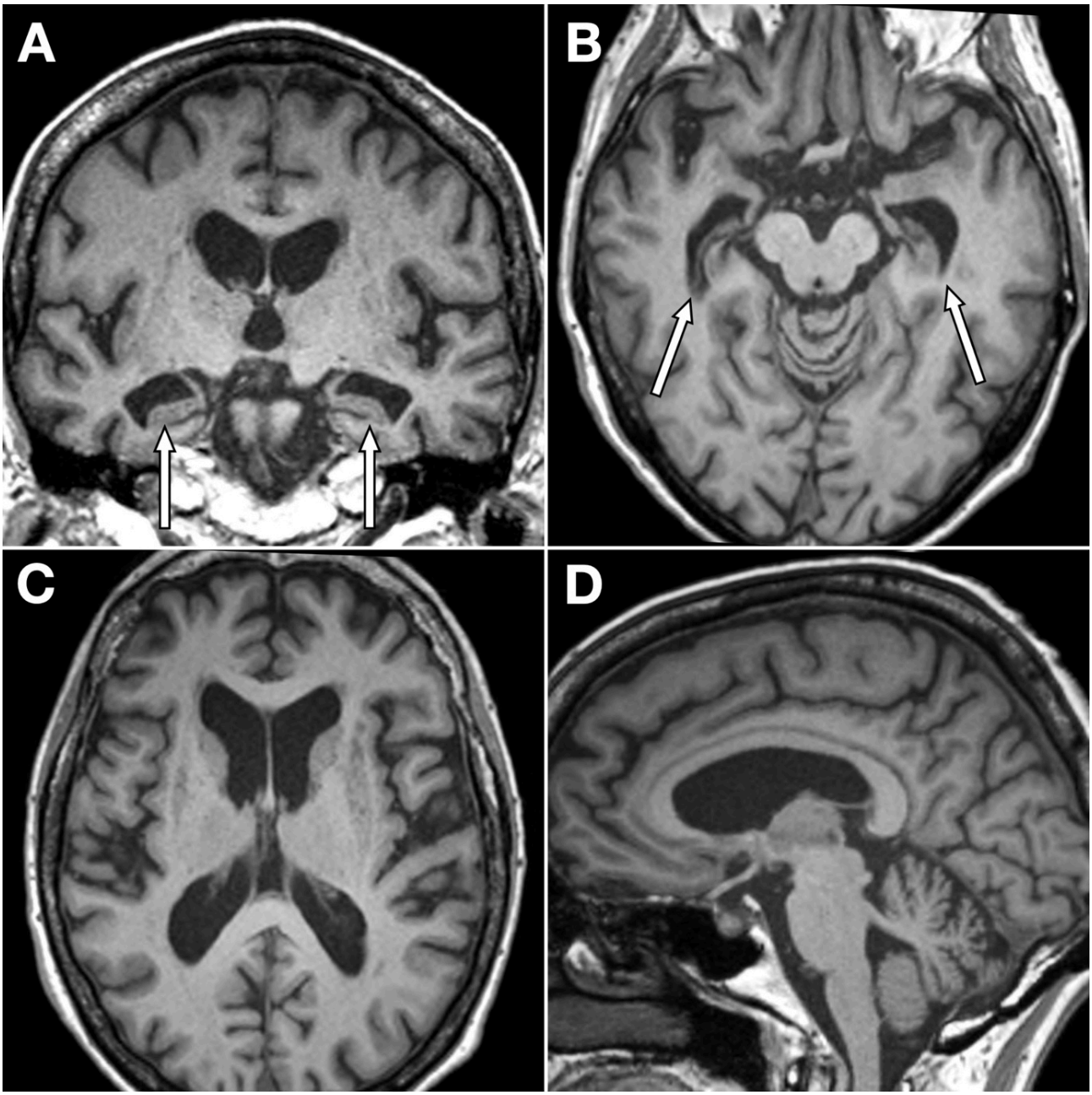


Figure 1. Alzheimer disease. Bilateral symmetrical hippocampal atrophy (white arrows) (panels A and B) with compensatory enlargement of the temporal horns of the lateral ventricles, with panels C and D showing global volume loss and sulcal widening.

Case courtesy of Frank Gaillard, Radiopaedia.org, rID 22196 (https://radiopaedia.org/cases/22196).

the advent of amyloid-targeted therapies: diffuse cortical amyloid plaques are seen more than a decade prior to established atrophy or symptom onset[16], and extent of plaque reduction throughout anti-amyloid treatment predicts clinical response[17].

Alzheimer disease variants

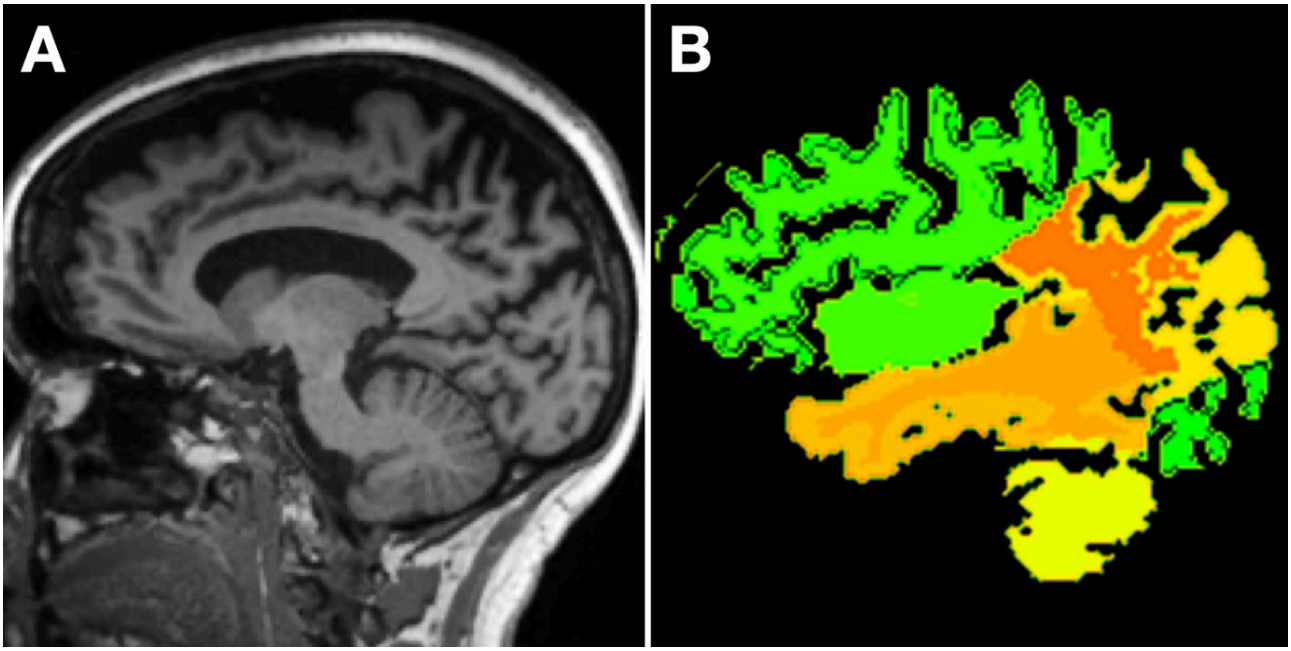


Figure 2. Posterior cortical atrophy. (**A**) Sagittal T1 imaging demonstrating parietal and occipital cortical atrophy, with (**B**) matching volume loss on quantitative morphometry.

Case courtesy of Gabrielle Matta, Radiopaedia.org, rID 47892 (https://radiopaedia.org/cases/47892).

Clinical variants of AD demonstrate different morphological patterns of atrophy. In patients presenting with visuospatial or apraxic deficits, the findings of parieto-occipital predominant atrophy with relatively preserved mesial temporal volume would point towards posterior cortical atrophy[18]. Compared to individuals presenting in older age, early onset AD (<65 years) tends to demonstrate more pronounced and widespread involvement of the neocortex, particularly involving the parietotemporal cortices[19]. Familial forms of AD, such as those related to *presenilin* mutations (e.g. PSEN1/2, APP), show characteristic early involvement of the deep grey matter structures (striatum, thalamus)[20]. *Limbic-predominant age-related TDP-43 encephalopathy (LATE)*

LATE is a common neurodegenerative disorder in the elderly that pathologically manifests as TDP-43 proteinopathy in limbic system structures such as the hippocampus[21]. Medial temporal lobe hypometabolism and volume loss is the main feature, typically beginning in the amygdala and progressing posteriorly to involve the hippocampus. The main differential for LATE is Alzheimer's disease, which can also co-exist. Both conditions demonstrate medial temporal lobe hypometabolism and volume loss with amyloid and tau PET studies being supportive of LATE. Additionally, the rate of hippocampal atrophy is faster in LATE and more commonly asymmetric compared to Alzheimer's disease[21].

Amyloid related pathology

In roughly a quarter of Alzheimer's disease cases[22], atrophy co-exists with the imaging findings of cerebral amyloid angiopathy – namely, lobar microhaemorrhages, superficial siderosis and white matter disease secondary to amyloid plaque accumulation in small vessel walls[23]. Identifying features of CAA can increase confidence in

diagnosing ADin cases of mild atrophy, but importantly requires exclusion of other aetiologies of haemorrhagic disease (e.g. trauma, lesional haemorrhage, hypertension).

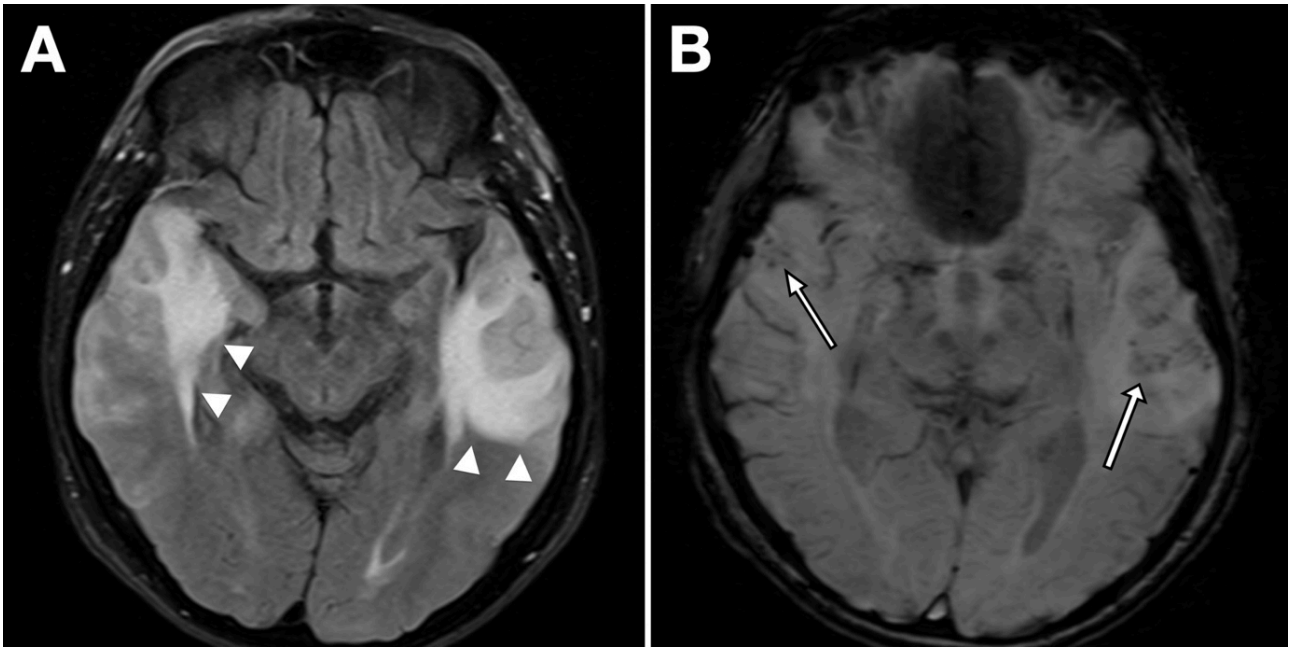


Figure 3. Amyloid related pathology. (**A**) FLAIR hyperintense parenchymal edema seen in ARIA-E (white arrow heads). (**B**) Scattered microhaemorrhages which were new compared to baseline imaging seen in ARIA-H (white arrows).

Case courtesy of Rodrigo Dias Duarte, Radiopaedia.org, rID 147243 (https://radiopaedia.org/cases/147243).

The imaging findings of CAA and amyloid related inflammation or angiitis overlap with those of amyloid-related imaging abnormalities (ARIA) in patients on amyloid-targeting therapies such as lecanemab and donanemab. ARIA are characterised by development of new parenchymal andsulcal FLAIR and SWI signal changes compared to baseline imaging. These changes are most often found in asymptomatic patients during routine monitoring, but occasionally patients may be symptomatic with headache, nausea or new neurological impairment[24 25]. The imaging findings are crucial to guiding management, as moderate or severe ARIA findings even in asymptomatic patients requires cessation or pausing of therapy[26].

Table 3: MRI findings in ARIA (Hampel 2023)

ARIA Type	Mild	Moderate	Severe
ARIA-E	FLAIR hyperintensity confined to sulcus and/or cortex/subcortex white matter in one location 5 cm	FLAIR hyperintensity 5-10 cm in single greatest dimension, OR multiple sites each measuring <10 cm	FLAIR hyperintensity >10 cm with associated gyral swelling and sulcal effacement. One or more separate/independent sites of involvement may be noted
ARIA-H (microhemorrhage)	≤4 new incident microhemorrhages	5-9 new incident microhemorrhages	≥10 new incident microhemorrhages
ARIA-H (superficial siderosis)	1 focal area of superficial siderosis	2 focal areas of superficial siderosis	>2 areas of superficial siderosis

Vascular dementia

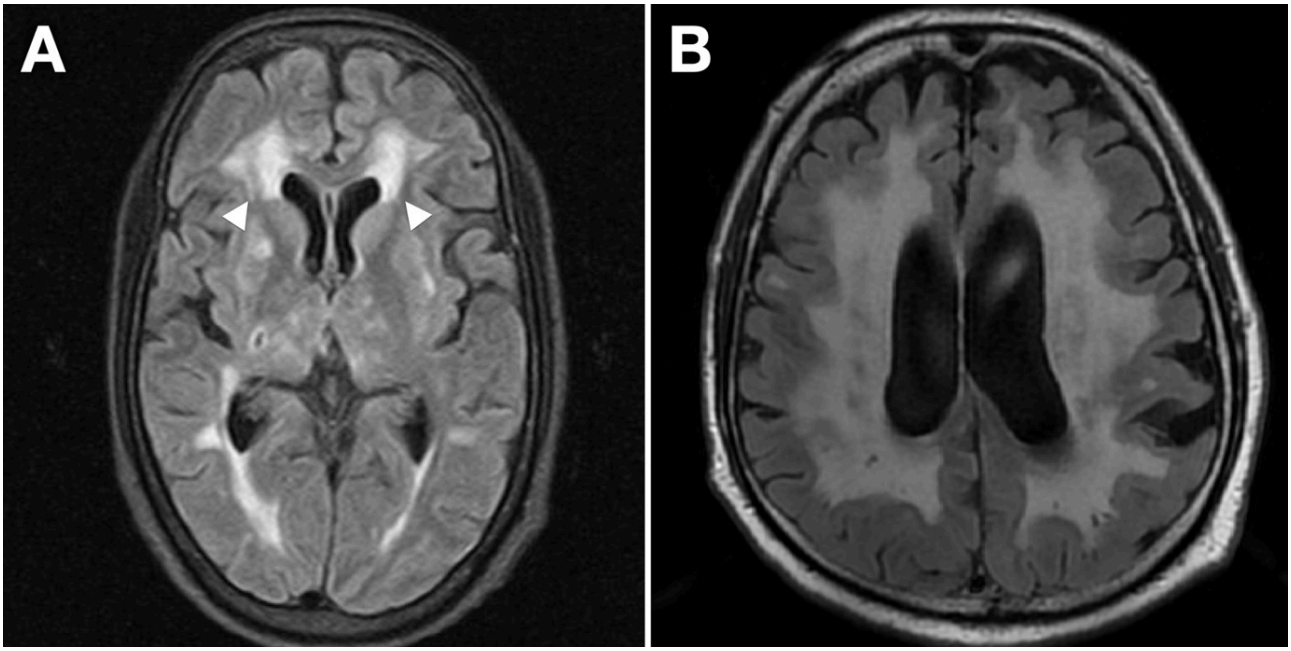


Figure 4. Vascular Dementia. (**A**) Periventricular white matter disease (white arrow heads) and scattered lacunar infarcts in a patient presenting with cognitive impairment. (**B**) Confluent periventricular white matter disease extending to the subcortex in a separate case.

*Image (**A**) courtesy of Jignesh Modi, Radiopaedia.org, rID 32829 (https://radiopaedia.org/cases/32829). Image (**B**) courtesy of Himel Kumar Biswas, Radiopaedia.org, rID 227874 (https://radiopaedia.org/cases/227874).*

Key structural findings (MRI)	Periventricular and subcortical white matter FLAIR hyperintensity [27] Lacunar and cortical infarcts Diffuse atrophy
Nuclear medicine	FDG PET: ↓ corresponding to vascular territories, cortical and subcortical distribution, ↓ at sites of prior vascular insult. Changes may appear patchy. May co-exist with AD (or non-AD) pattern of metabolism in mixed dementia [28]
Radiological grading	Fazekas (white matter disease)
Pitfalls	Other diffuse white matter diseases Lobar microhaemorrhages and superficial siderosis may be more in keeping with CAA

Vascular dementia encapsulates several related conditions, characterised by repeated or chronic vascular insults to the brain in the setting of arteriosclerosis, affecting both grey and white matter structures. Imaging findings range from diffuse periventricular white matter FLAIR hyperintensities (subcortical arteriosclerotic encephalopathy), to multiple cortical infarcts, to lacunar ‘strategic’ infarcts of the thalamus and basal forebrain which can result in disproportionate degrees of cognitive impairment [29]. The extent of cortical atrophy can therefore vary, from diffuse to focal depending on the specific insult. There are often associated microhaemorrhages in a deep or subcortical distribution [30]. FDG-PET hypometabolism often involves the frontal lobes and deep nuclei [28]. Vascular pathology frequently co-exists with Alzheimer disease or other neurodegenerative conditions, with multiple shared risk factors between conditions, requiring clinical differentiation as to the dominant disease process [31].

Frontotemporal lobar degeneration

Key structural findings (MRI)	Frontal and temporal lobe atrophy, often asymmetric with greater involvement on the left corresponding to language areas [32]
Supportive findings	Preserved mesial temporal volume

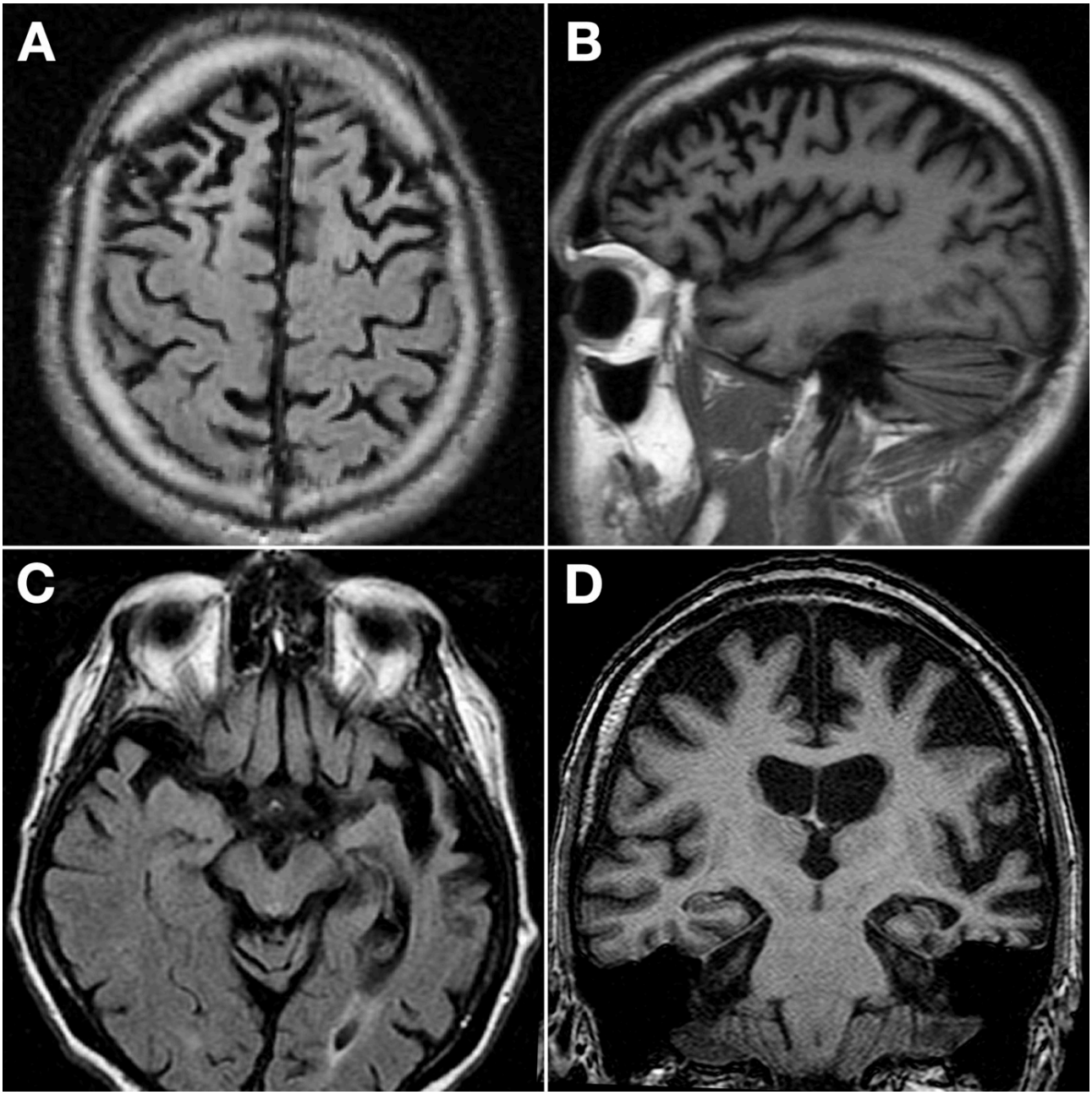


Figure 5. Frontotemporal lobar degeneration (FTLD). (**A** and **B**) Bilateral frontal lobar atrophy in a patient with behaviour variant FTLD. (**C** and **D**) Severe left temporal pole, operculum and parietal atrophy in a patient with language variant FTLD.

Images (A and B) courtesy of Frank Gaillard, Radiopaedia.org, rID 28163 (https://radiopaedia.org/cases/28163). Image (C and D) courtesy of Brad Hayhow, Radiopaedia.org, rID 22365 (https://radiopaedia.org/cases/22365).

Nuclear medicine	FDG PET: ↓ frontal association cortex, anterior temporal lobe, caudate nucleus, thalamus. Asymmetry common. Additionally, variants may demonstrate: • bvFTD: ↓ frontal and anterior temporal cortices, caudate nucleus • svFTD: ↓ anterior temporal cortex (left >> right) • nfvFTD: ↓ left posterolateral and superomedial frontal cortex, left insula Amyloid PET: Typically normal
Variants	bvFTD: Bilateral frontal lobe involvement svFTD: Left temporal lobe involvement (particularly temporal pole) nfvFTD: Left frontal operculum (Broca's area) and left insula involvement

bvFTD – behavioural variant FTD; svFTD – semantic variant FTD; nfvFTD – non-fluent variant FTD.

Structural imaging in frontotemporal dementias will show varying degrees of frontal and temporal lobar volume loss depending on the subtype, typically with a younger age of presentation than Alzheimer disease (40-60s). The classic appearance of 'knife-like gyri' secondary to severe atrophy is a late finding. In cases of diagnostic uncertainty or in early disease, frontotemporal hypometabolism on FDG PET without involvement of areas more characteristic of AD such as the posterior cingulate cortex, and negative amyloid PET, can assist in differentiating from Alzheimer syndromes[8].

Dementia with Lewy Bodies

Key structural findings (MRI)	Non-specific atrophy Loss of the swallow tail appearance of the substantia nigra is also described in DLB (as well as Parkinson Disease) [33].
Supportive findings	Normal appearance of the mesial temporal lobes and hippocampi is useful in distinguishing DLB from AD [34] [35] [1] Compared to Parkinson disease dementia, there is a higher likelihood of concomitant cerebral amyloid angiopathy and small vessel ischaemic changes [36].
Nuclear medicine	FDG PET: May appear similar to AD, however reduced uptake in the occipital cortex is more suggestive of DLB. Preserved metabolism in the posterior cingulate gyrus ('cingulate island sign') [37] [38] [39]. I-123 Ioflupane SPECT (DaTscan) • Loss of the comma shape of the corpus striatum, appearing more oval or round, may be more symmetric compared to Parkinson disease [36]. • An abnormal DaTscan is useful in distinguishing DLB from AD especially when clinical and FDG-PET findings are indeterminate [40]. Amyloid PET: Positive in >50% of patients [41]

Structural imaging is nonspecific in DLB, however the relative preservation of mesial temporal lobe and neocortical volumes is helpful in excluding differential diagnoses such as AD. Nuclear medicine studies may be more useful, particularly in demonstrating reduced nigrostriatal uptake of dopamine-transporter targeted tracers, which is 88% sensitive and 100% specific for differentiation with non-Lewy body dementias [42].

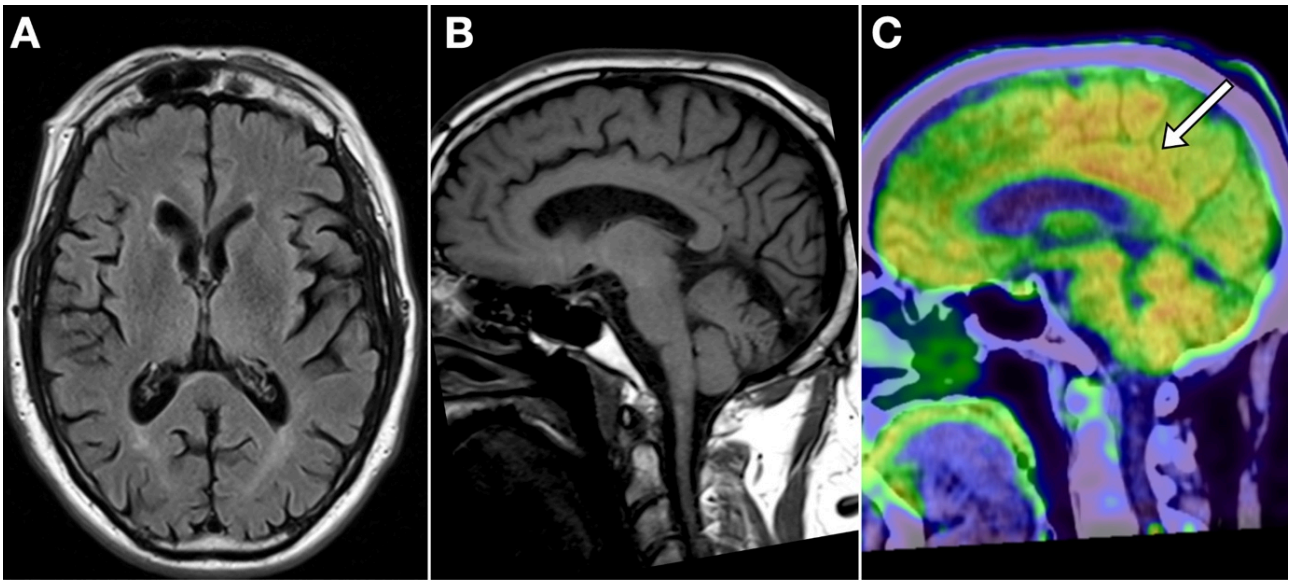


Figure 6. Dementia with Lewy Bodies (DLB). (**A** and **B**) Non-specific mild generalised parenchymal volume loss. (**C**) Spared metabolism in the posterior aspect of the cingulate sulcus (white arrow) on PET/CT (cingulate island sign).

Case courtesy of Shisheng Lu, Radiopaedia.org, rID 93603 (https://radiopaedia.org/cases/93603).

Parkinson disease and Parkinson-Plus Syndromes

Parkinson Disease

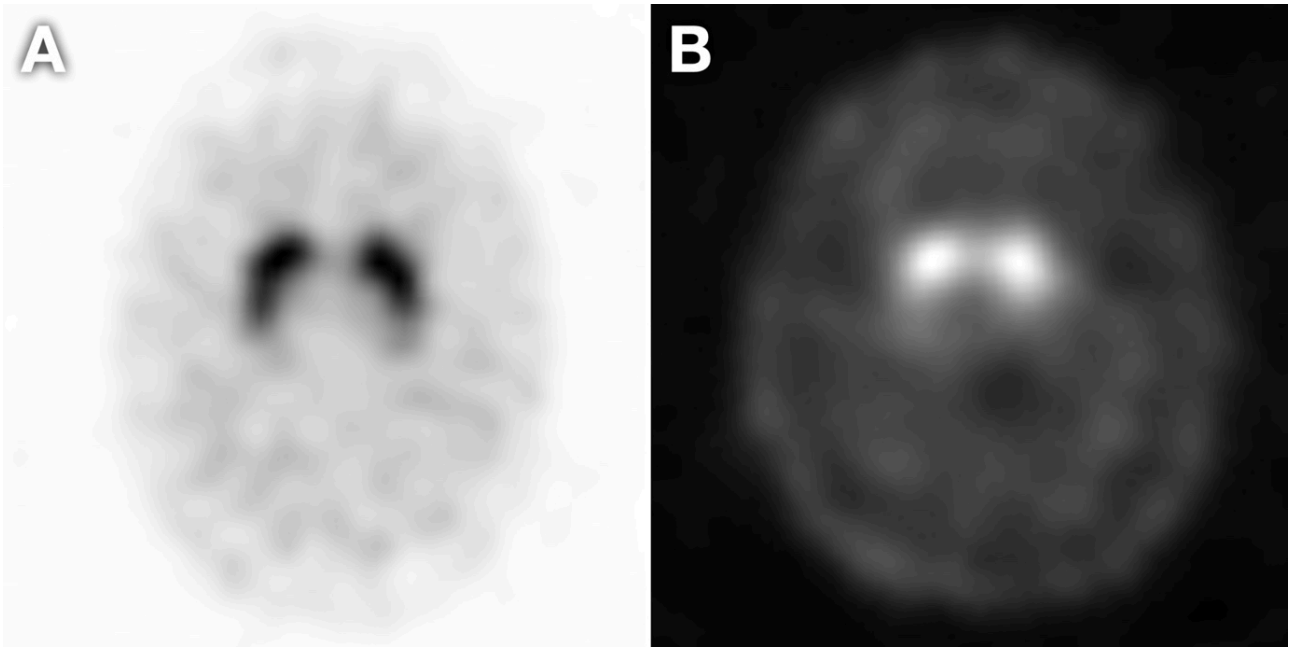


Figure 7. Parkinson Disease (PD). (**A**) Normal DaTscan for comparison. (**B**) Loss of the comma-shaped appearance of the corpus striatum on DaTscan.

Image (A) courtesy of Austin Patrick, Radiopaedia.org, rID 173581 (https://radiopaedia.org/cases/173581). Image (B) courtesy of Stefan Lazic, Radiopaedia.org, rID 158505 (https://radiopaedia.org/cases/158505).

Key structural findings (MRI)	Limited, with no reliable structural findings currently in use. Loss of the normal swallow tail appearance in the substantia nigra is a promising diagnostic sign but not possible to apply reliably at the moment [33].
Nuclear medicine	VMAT2/FDOPA PET: ↓ corpus striatum (particularly dorsal putamen) FDG PET: ↓ parieto-occipital and premotor cortices, preserved or relatively ↑ in cerebellum, pons, thalamus, lentiform nucleus [43]. I-123 Ioflupane SPECT (DaTscan): Loss of the comma shape of the corpus striatum, appearing more oval or round [1].
Variants	Idiopathic: Typically encountered in elderly patients Young Onset: Manifesting before 50 years of age Juvenile: Manifesting before 21 years of age

Similar to DLB, structural imaging has a limited role in the diagnosis of Parkinson disease with no consistently demonstrated patterns of regional atrophy. Loss of the normal 'swallow tail' appearance of the substantia nigra on T2* sequences has been described [44] but is of variable utility in day to day practice due to motion artefact, variable identification depending on magnet strength [33], and overlap with other neurodegenerative syndromes [45]. The main role of structural imaging in patients with Parkinsonism is to look for features of Parkinson-plus syndromes such as multiple systems atrophy and progressive supranuclear palsy. Nuclear medicine findings overlap with those of DLB, requiring clinical differentiation as to the predominance and onset of cognitive vs motor symptoms.

Multiple System Atrophy

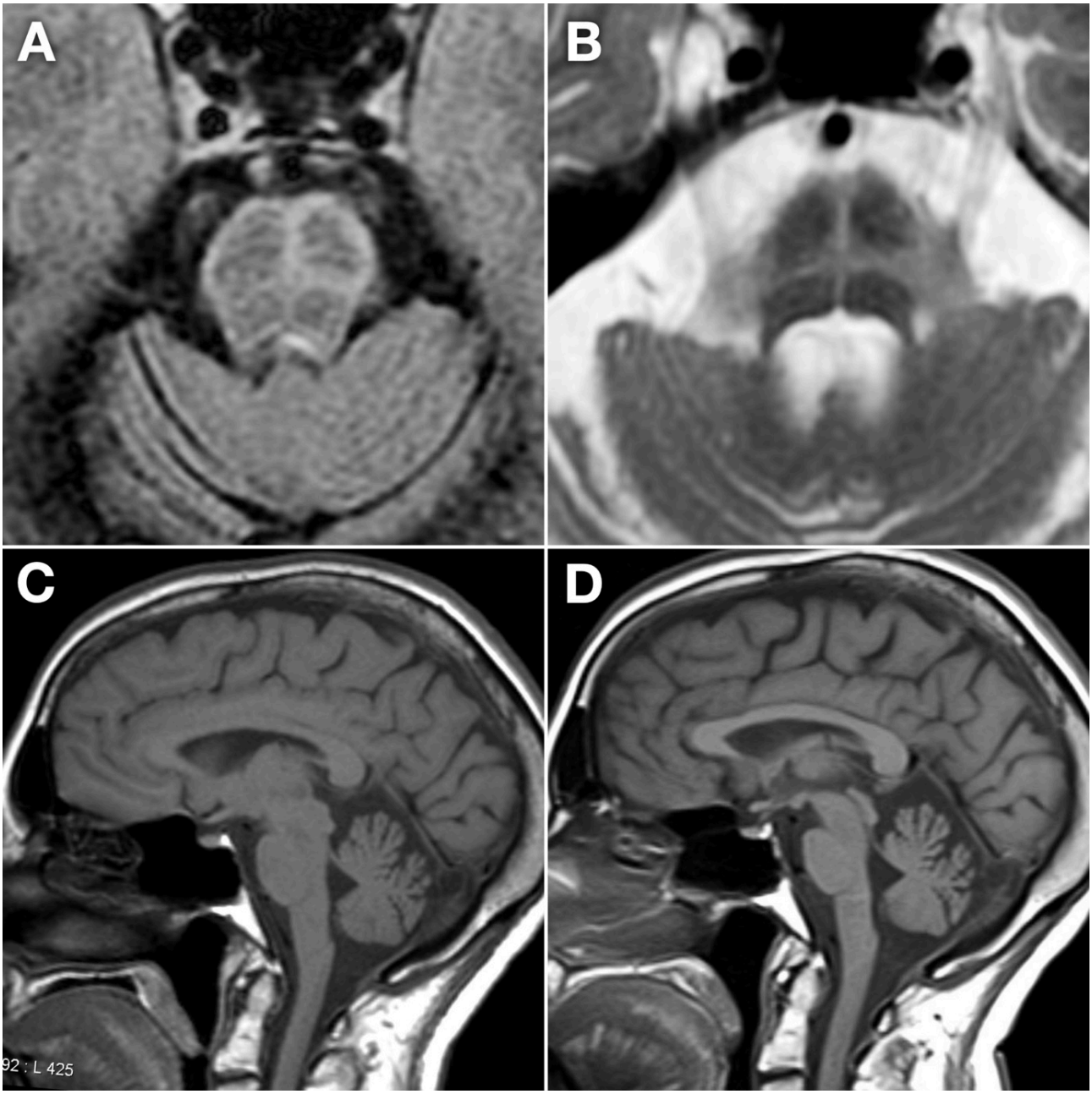


Figure 8. Multiple systems atrophy cerebellar subtype (MSA-C). (**A** and **B**) Increased FLAIR and T2 signal in the pons (hot cross bun sign). (**C** and **D**) Scans six months apart showing progressive atrophy of the pons and cerebellum in a separate case.

Cases courtesy of Frank Gaillard, Radiopaedia.org, rID 5465 and 22188 (https://radiopaedia.org/cases/5465 and https://radiopaedia.org/cases/22188).

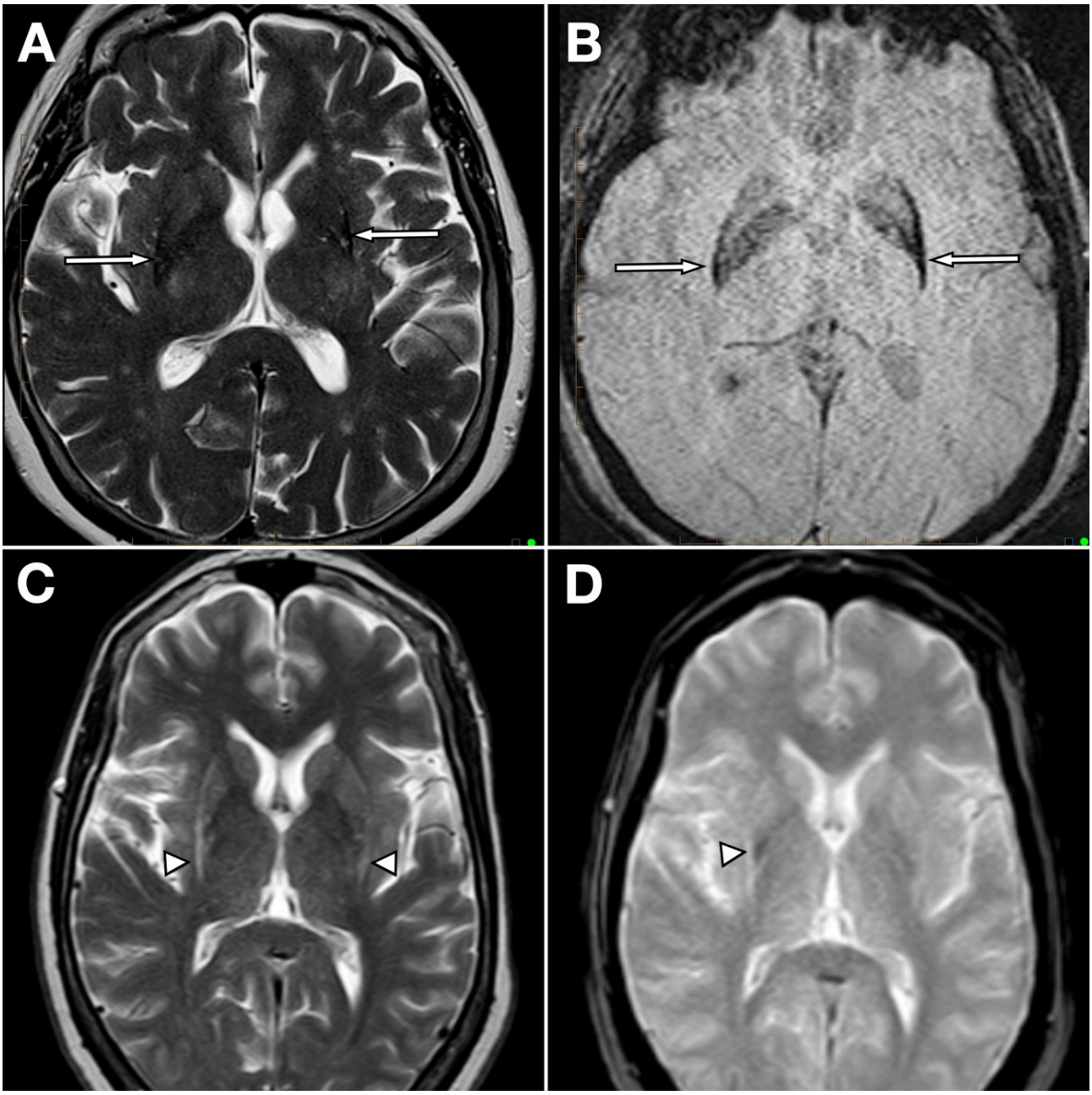


Figure 9. Multiple system atrophy parkinsonian subtype (MSA-P). (**A**) Reduced putaminal T2 signal (white arrows). (**B**) Bilaterally reduced putaminal signal on SWI (white arrows), particularly evident along the lateral aspect. (**C**) Bilaterally increased T2 signal along the lateral aspect of the putamen, the putaminal rim sign (white arrows heads) with (**D**) subtle signal loss in the right putamen on gradient echo sequence (white arrow head).

Images (A and B) courtesy of Wen Jak Ma, Radiopaedia.org, rID 71750 (https://radiopaedia.org/cases/71750). Images (C and D) courtesy of Dalia Ibrahim, Radiopaedia.org, rID 228282 (https://radiopaedia.org/cases/228282).

Key structural findings (MRI)	Atrophy of putamen (and signal decrease on iron-sensitive sequences), middle cerebellar peduncle, pons and cerebellum [46]. Hot-cross bun sign
Nuclear medicine	FDG PET: ↓ putamen (MSA-C < MSA-P), ↓ cerebellum and brainstem (MSA-C > MSA-P) [43] DaTscan: ↓ and often asymmetric striatal uptake resulting in loss of the normal “comma shape” [1]

Pitfalls	There is significant overlap of MRI findings between MSA-C and MSA-P with the distinction being the clinically-predominant motor syndrome [46]. Be careful not to mistake small vessel ischaemia in the pons for the hot-cross bun sign. T2 high signal microvascular ischaemia can spare the central pons, creating the appearance of a cross. However, the cross will appear as low signal relative to the remainder of the pons, in contrast to a true hot-cross bun sign where the cross is high on T2. Figure 9 shows high T2 signal on the outer margin of the putamen, a sign described in MSA. It is worth noting that this can be seen in normal cases on 3 Tesla MRI [47]. Be wary only to consider describing this finding on a 1.5 Tesla MRI.

Progressive Supranuclear Palsy

Key structural findings (MRI)	Midbrain atrophy [48] • Raised magnetic resonance parkinsonism index (MRPI): **(P/M) x (MCP/SCP)** *MCP = average width of the middle cerebellar peduncles* *SCP = average width of the superior cerebellar peduncles* *P = area of pons in midsagittal plane* *M = area of midbrain in midsagittal plane* • Midbrain to pons area ratio: ◦ Normal = ~0.24 ◦ PSP = ~0.12 [49] • Hummingbird sign: Characteristic appearance in midsagittal plane due atrophy of the midbrain and flattening of the superior contour of the midbrain [50]. • Mickey mouse sign: Reduction of anteroposterior midline midbrain diameter at the level of the superior colliculi on axial imaging (interpeduncular fossa to the intercollicular groove: <12mm) [51]. Frontal lobe volume loss
Nuclear medicine	FDG PET: ↓ basal ganglia, thalamus, midbrain, anterior cingulate gyrus, prefrontal area [43] DaTscan: ↓ and often asymmetric striatal uptake resulting in loss of the normal “comma shape” [1]
Pitfalls	The imaging features in PSP are non-specific and it is important that the reported measurements are only applied in cases where the aim is to distinguish PSP from another movement disorder. If applied outside of this context, it is likely to lead to false positives and introduce confusion to cases. The hummingbird sign and mickey mouse signs must be reported with caution as normal studies frequently have similar subjective appearances.

Progressive supranuclear palsy is a neurodegenerative disease characterized by decreased cognition, abnormal eye movements (supranuclear vertical gaze palsy), postural instability and fall, parkinsonism and speech disturbance. The role of imaging in this disease is to help distinguish PSP from other movement disorders such as Parkinson disease, multiple system atrophy and corticobasal degeneration [51]. The imaging features in PSP are non-specific and it is important that they are only applied in the appropriate clinical context, helping distinguish PSP from other movement disorders [49].

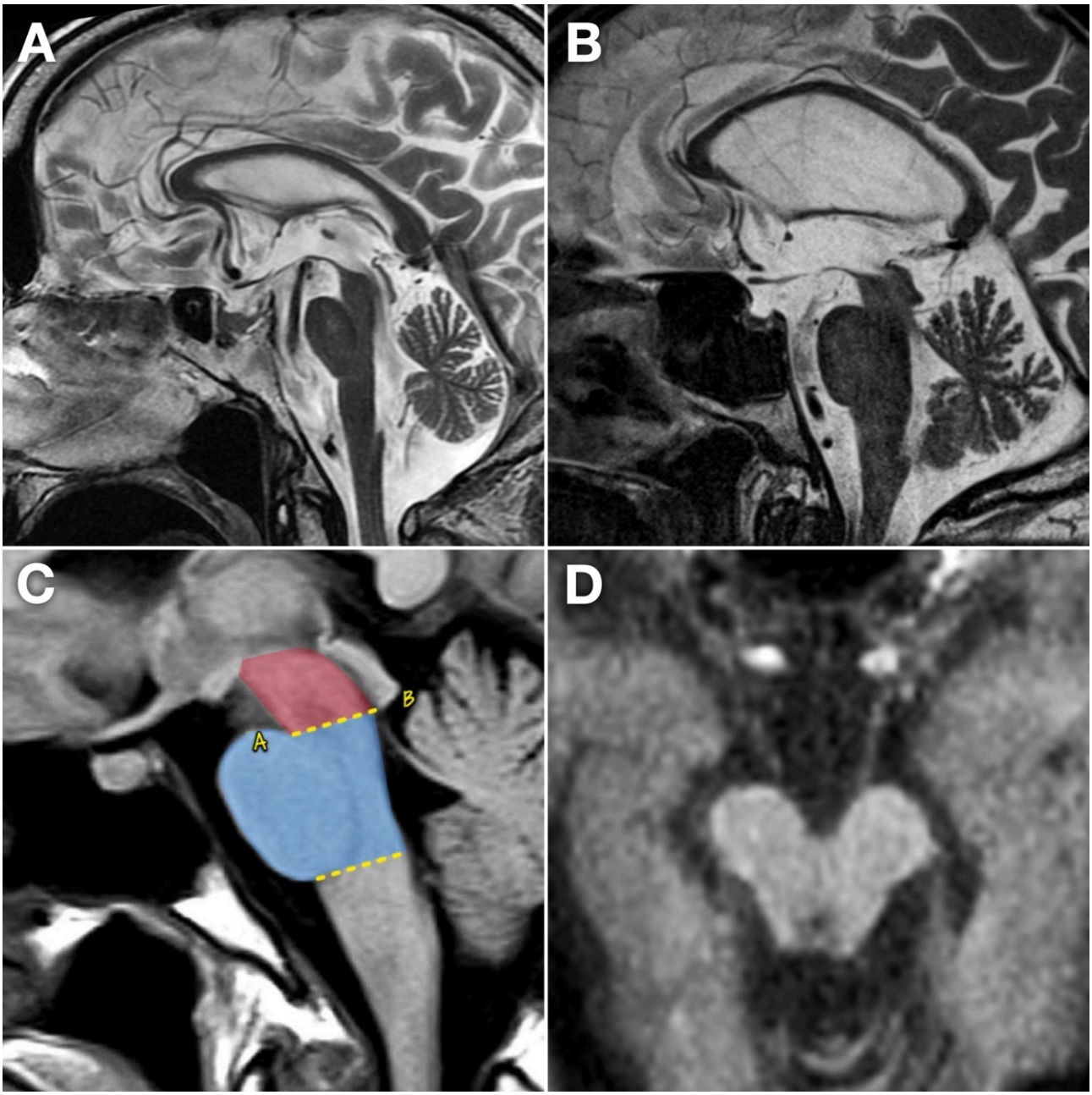


Figure 10. Progressive supranuclear palsy (PSP). (**A** and **B**) Midbrain atrophy with associated hummingbird sign. (**C**) Calculation of the midbrain (red highlight) to pons (blue highlight) area ratio. (**D**) Midbrain atrophy with associated mickey mouse sign.

Image (A) is courtesy of Prashant Gupta, Radiopaedia.org, rID 18863 (https://radiopaedia.org/cases/18863). Images (B and C) courtesy of Frank Gaillard, Radiopaedia.org, rID 34458 and 27991 (https://radiopaedia.org/cases/34458 and https://radiopaedia.org/cases/27991). Image (D) courtesy of Roberto Schubert, Radiopaedia.org, rID 16914 (https://radiopaedia.org/cases/16914).

Corticobasal Degeneration

Key structural findings (MRI)	Asymmetric cortical atrophy. Superior parietal lobule atrophy is the most constant feature [52]. Atrophy can also involve the perirolandic gyri, precentral gyri, postcentral gyri and superior frontal gyri. Bilateral atrophy of the basal ganglia Atrophy of the corpus callosum T2 hyperintensity in the subcortical white matter of affected gyri and the posterolateral putamen
Nuclear medicine	FDG PET: ↓ frontoparietal cortex (particularly inferior parietal lobule), thalamus, caudate nucleus. Typically asymmetric and contralateral to the clinically affected side [43]. DaTscan: ↓ and often asymmetric striatal uptake resulting in loss of the normal “comma shape” [1]
Pitfalls	Corticobasal degeneration refers to a subset of cases confirmed as a tauopathy pathologically. Corticobasal syndrome is the clinical syndrome. In addition to corticobasal degeneration, corticobasal syndrome can also be caused by progressive supranuclear palsy (PSP-CBS), frontotemporal dementia, posterior cortical atrophy variant of Alzheimer disease, and Creutzfeldt-Jakob disease [53].

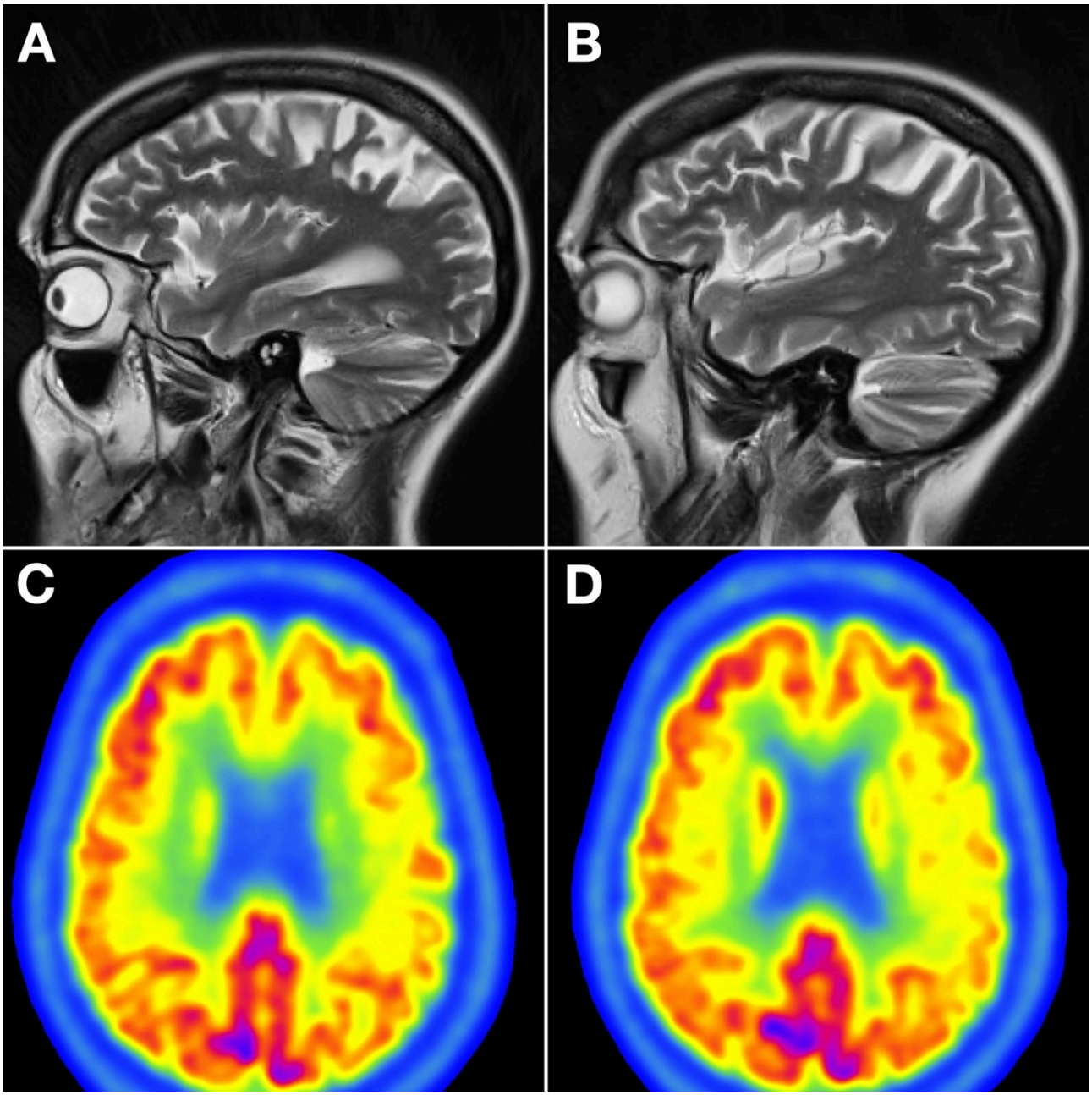


Figure 11. Corticobasal degeneration. (**A** and **B**) Disproportionate cerebral volume loss towards the vertex, predominantly affecting the parietal lobe, but also with frontal lobe involvement. (**C** and **D**) Hypometabolism in the left sensorimotor strip and left posterior frontal cortex on FDG PET.

Case courtesy of Stefan Lazic, Radiopaedia.org, rID 185756 (https://radiopaedia.org/cases/185756).

Multiple Sclerosis

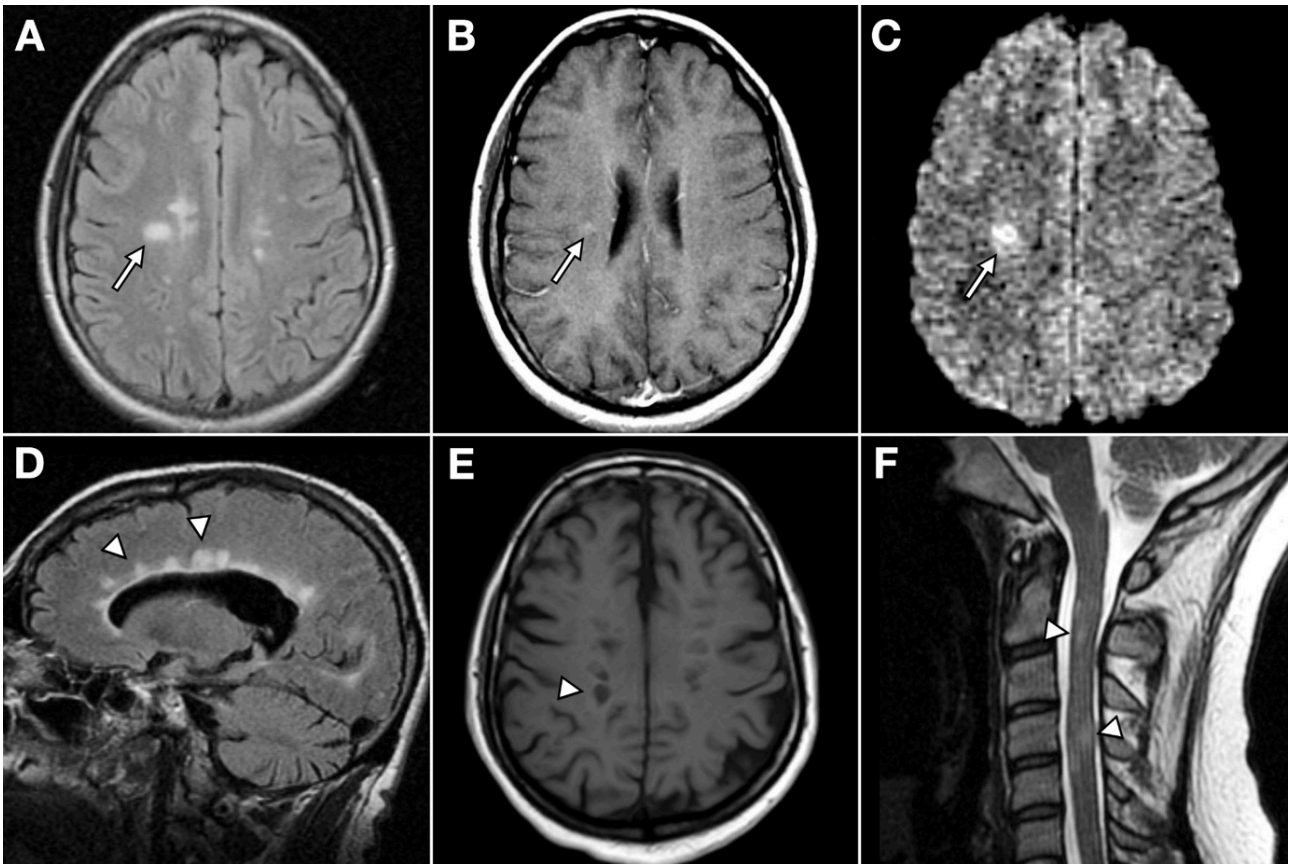


Figure 12. Multiple Sclerosis. (**A**) T2 hyperintense lesions perpendicular to the lateral ventricles with (**B**) corresponding enhancement and (**C**) diffusion restriction, consistent with active lesions. (**D**) "Dawson Fingers" morphology of periventricular lesions perpendicular to the lateral ventricles. (**E**) T1 hypointense "black holes" in the periventricular white matter. (**F**) Peripherally located T2 hyperintense lesions in the cervical cord.

Cases courtesy of Frank Gaillard, Radiopaedia.org, rID 35916, 2634, 2635 and 35195 (https://radiopaedia.org/cases/35916, https://radiopaedia.org/cases/2634, https://radiopaedia.org/cases/2635 and https://radiopaedia.org/cases/35195).

Key structural findings (MRI)	Brain: Demyelination plaques typically occur in the periventricular, juxtacortical and infratentorial regions but can also be found in the cortices and deep white matter[54]. Lesions are T2/FLAIR hyperintense. If active, there may be surrounding oedema, contrast-enhancement and diffusion restriction. FLAIR is more sensitive for periventricular and juxtacortical lesions while T2 is more sensitive for infratentorial lesions. • Ependymal dot-dash sign; Small dots of FLAIR high signal in the inferior corpus callosum representing early perivenular involvement[55]. • Dawson's fingers; FLAIR high signal perpendicular to the lateral ventricles as the perivenular involvement propagates along the periventricular medullary veins. • On T1, hypointense "black holes" develop in the chronic stage, representing irreversible neuronal loss. • Optic nerve lesion may also be seen as T2/FLAIR hyperintensity. • Brain atrophy; Best appreciated with volumetric analysis such as MR Morphometry. The degree of brain atrophy by volumetric analysis correlates to the degree of disability[56]. The degree of cortical atrophy correlates to the degree of cognitive dysfunction. Spinal cord: Lesions are typically in the periphery and are less than three segments in craniocaudal dimension[57]. Signal is increased on T2 and inversion recovery sequences.
Nuclear medicine	Not typically used in this condition.
Radiological grading	McDonald's criteria
Pitfalls	In the cord, centrally-located lesions or longitudinally extensive lesions (longer than three segments) are atypical and suggest another demyelinating condition such as neuromyelitis optica[57].

Traumatic Brain Injury

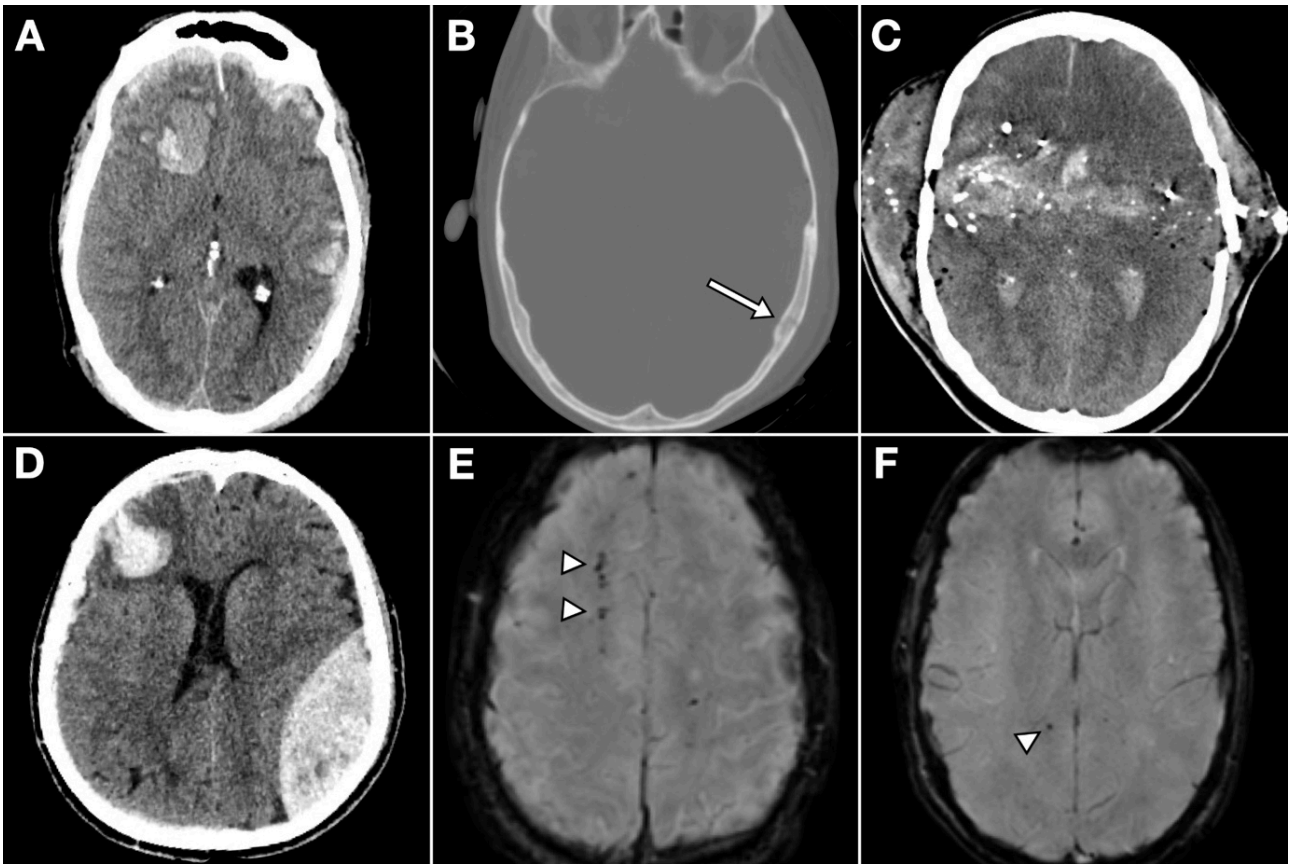


Figure 13. Multiple cases of traumatic brain injury. (**A**) Closed head injury with multiple right frontal and left temporal haemorrhagic contusions, bifrontal subdural haematomas and (**B**) corresponding left temporal bone skull fracture (white arrow). (**C**) Penetrating gunshot head injury (right-to-left bullet transit) with entry and exit skull fractures, pneumocephalus, bullet fragments, haemorrhage in the ventricles and diffuse cerebral oedema. (**D**) Closed head injury with a right frontal haemorrhagic contusion and an extradural haematoma overlying the left temporal and parietal lobes. Hypodense foci within the extradural haematoma suggests hyperacute haemorrhage. (**E** and **F**) Closed head injury with multiple microhaemorrhages at the grey-white matter junction and in the posterior corpus callosum (white arrow heads), consistent with diffuse axonal injury grade 2.

Images (A and B) courtesy of Derek Smith, Radiopaedia.org, rID 36667 (https://radiopaedia.org/cases/36667). Image (C) courtesy of Sajoscha A. Sorrentino, Radiopaedia.org, rID 14487 (https://radiopaedia.org/cases/14487). Image (D) courtesy of Emma Gevorgyan, Radiopaedia.org, rID 203818 (https://radiopaedia.org/cases/203818). Images (E and F) courtesy of Henry Knipe, Radiopaedia.org, rID 44683 (https://radiopaedia.org/cases/44683).

Key structural findings [58]	CT:
	• Skull fractures.
	• Parenchymal contusional haemorrhage, extradural and subdural haematomas and traumatic subarachnoid haemorrhage.
	• Subdural hygromas.
	• Characterising secondary mass effect such as midline shift (subfalcineherniation), uncal herniation, tonsillar herniation and hydrocephalus.
	• Cerebral oedema; Usually occult in mild cases.
	• Vascular injuries: Assessed with CT angiography. Both closed and penetrating mechanisms can result in vascular injuries including dissection, pseudoaneurysm formation and transection.
	• Assessing the mechanism and extent of penetrating injuries. Can assess entry and exit sites for gunshots, the depth of injury in stabbing and for residual bullet or weapon fragments.
	• Assessment of gliosis and encephalomalacia following the acute phase.
	
	MRI:
	• The main role is the assessment for diffuse axonal injury[58]. The typical scenario is a closed head injury with clinical severity out of proportion to the imaging findings.
	  ◦ Grade 1: Grey-white junction only.
	  ◦ Grade 2: Involves the corpus callosum.
	  ◦ Grade 3: Involved the brain stem.
	• Increased sensitivity in identifying blood products in the acute setting.
	• Assessment of gliosis and encephalomalacia following the acute phase.

Nuclear medicine	Not typically used in this condition.
Pitfalls	In patients following a closed head injury with clinical findings out of proportion to the initial CT findings, it is important to consider pathology that is not readily appreciated on CT. In this case, MRI should be performed to assess for diffuse axonal injury. Another thing to consider in patients with neurological findings that don't match the initial CT is carotid and vertebral vascular injuries, which can occur in both closed and penetrating trauma [59]. CT angiography is increasingly being performed in the acute setting to assess for this.

The spectrum of imaging findings in traumatic brain injury is highly variable depending on mechanism and energy [58]. Broadly speaking, closed injuries (motor vehicle accidents, assault, sports injuries) may result in an initial 'coup' injury (e.g. skull fracture, subarachnoid haemorrhage, epidural haematoma at the point of contact); a 'contre-coup' injury through the contralateral brain surface contacting the inner table of the skull (e.g. basal temporal and frontal parenchymal contusions); and, depending on the severity, damage to the intervening tissues through shearing or deceleration mechanisms (e.g. diffuse axonal injury). Penetrating injuries (gunshots, stab wounds) result in tissue injury directly through the involved trajectory, as well as indirectly to surrounding tissues through dispersal of kinetic energy [60].

CT provides the vast majority of diagnoses in TBI, particularly in the acute setting, while MRI has a supplementary role in follow-up and prognostication with greater sensitivity for residual blood products, non-haemorrhagic contusions, and diagnosing diffuse axonal injury. Chronically,

gliosis and encephalomalacia may develop at a specific point of injury, as well as more generalised findings of cortical, hippocampal and white matter atrophy [61].

Motor Neuron Disease

Imaging features in Amyotrophic Lateral Sclerosis (ALS), the most common motor neuron disease

Key structural findings (MRI)	Imaging is normal in many cases. T2 hyperintensity may be seen in the corticospinal tracts in approximately 30% of cases [62]. GRE/SWI hypointensity may be seen in the cortex of the precentral gyrus (motor band sign) [63]. T1 hyperintensity can occasionally be seen in the tongue (bright tongue sign) representing fatty atrophy of the tongue due to chronic denervation (seen in patients with bulbar symptoms) [64].
Nuclear Medicine	Not typically used in this condition.
Pitfalls	It is important to recognise that imaging may be normal in ALS. The above described findings may be present and supportive of the diagnosis but a normal MRI does not rule out the diagnosis. It is common to see SWI hypointensity along the primary motor cortex in normal adults, which is thought to be due to age-related physiologic iron accumulation.

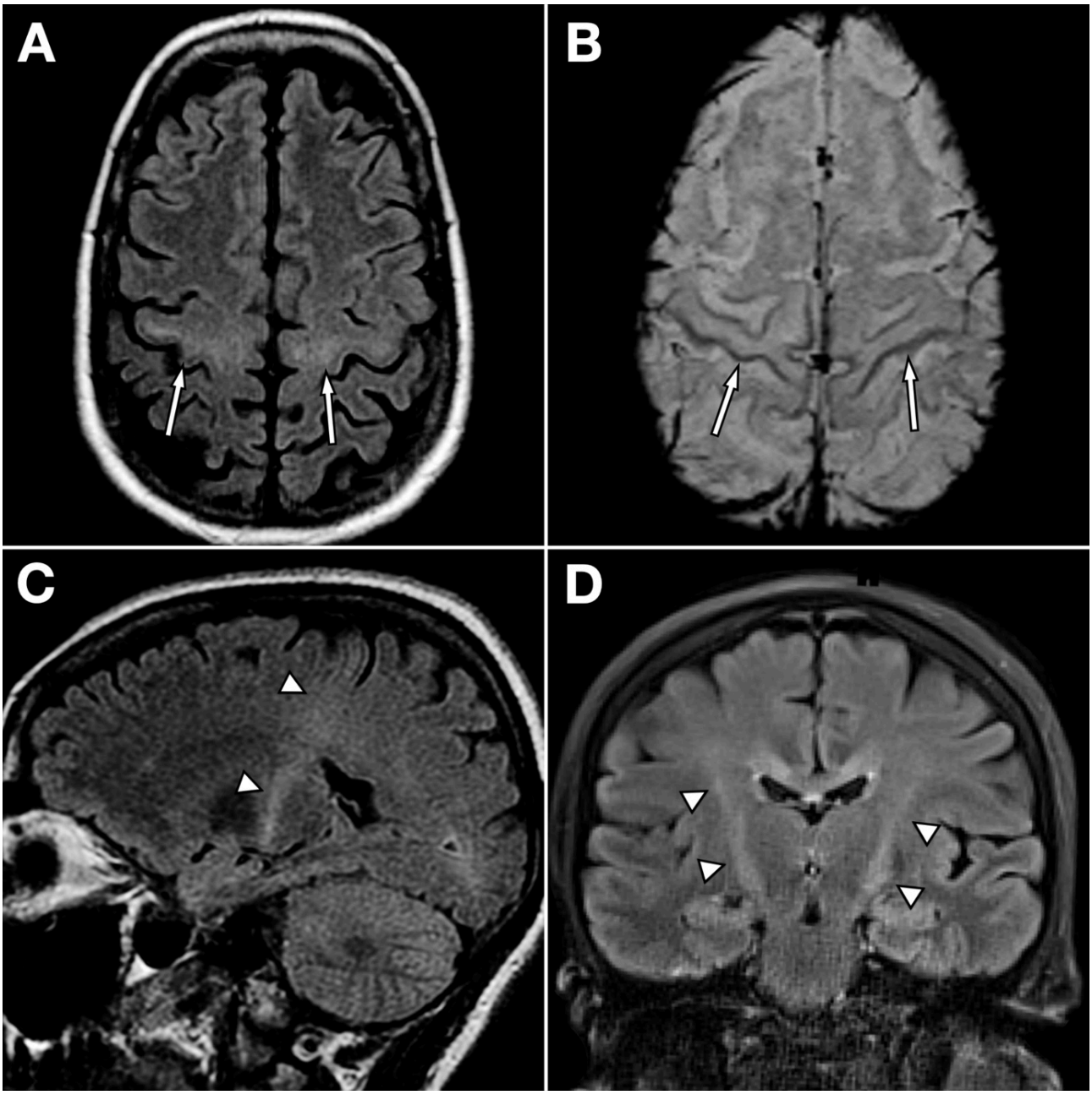


Figure 14. Amyotrophic Lateral Sclerosis. (**A**) Increased FLAIR signal in the precentral motor cortex bilaterally (white arrows) and (**B**) corresponding signal loss along the cortex of the precentral motor gyrus (white arrows) on susceptibility-weighted sequence (motor band sign). (**C** and **D**) Increased FLAIR signal from the precentral motor gyrus extending inferiorly along the corticospinal tracts through the posterior limb of the internal capsule (white arrow heads).

Images (A, B and C) courtesy of Frank Gaillard, Radiopaedia.org, rID 4717 and 4719 (https://radiopaedia.org/cases/4717 and https://radiopaedia.org/cases/4719). Image (D) courtesy of Yves Leonard Voss, Radiopaedia.org, rID 70821 (https://radiopaedia.org/cases/70821).

Disorders of the Deep Nuclei

Huntington Disease

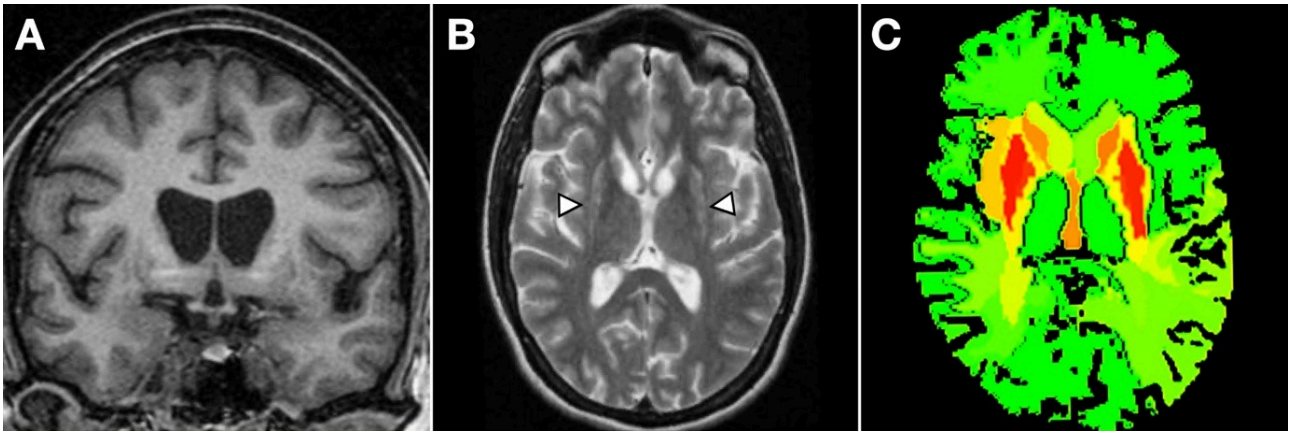


Figure 15. Huntington Disease. **(A** and **B**) Caudate nucleus atrophy and (**B**) putaminal atrophy (white arrow heads) with enlargement of the frontal horns of the lateral ventricles creating a “boxcar” appearance in the coronal plane (**A**). (**C**) Morphometry map showing caudate nucleus atrophy (orange) and putaminal atrophy (red).

Case courtesy of Frank Gaillard, Radiopaedia.org, rID 28732 and 55786 (https://radiopaedia.org/cases/28732 and https://radiopaedia.org/cases/55786).

Key structural findings (MRI)	Caudate head atrophy and putaminal atrophy (not as obvious on visual inspection but evident on morphometry) [65] [66] The combination of caudate head and putaminal atrophy causes enlargement of the frontal horns, creating a “box” or “box car” configuration . This can be quantified by two measurements: • Frontal horn width to intercaudate distance ratio (FH/CC) • Intercaudate distance to inner table width ratio (CC/IT) Reduced signal in the basal ganglia on T2 and SWI due to iron deposition. Generalised age-inappropriate cortical volume loss [67].
Nuclear medicine	FDG PET: ↓ caudate nucleus, putamen, and select cortical areas, even before discernible volume loss [43].

Wilson disease

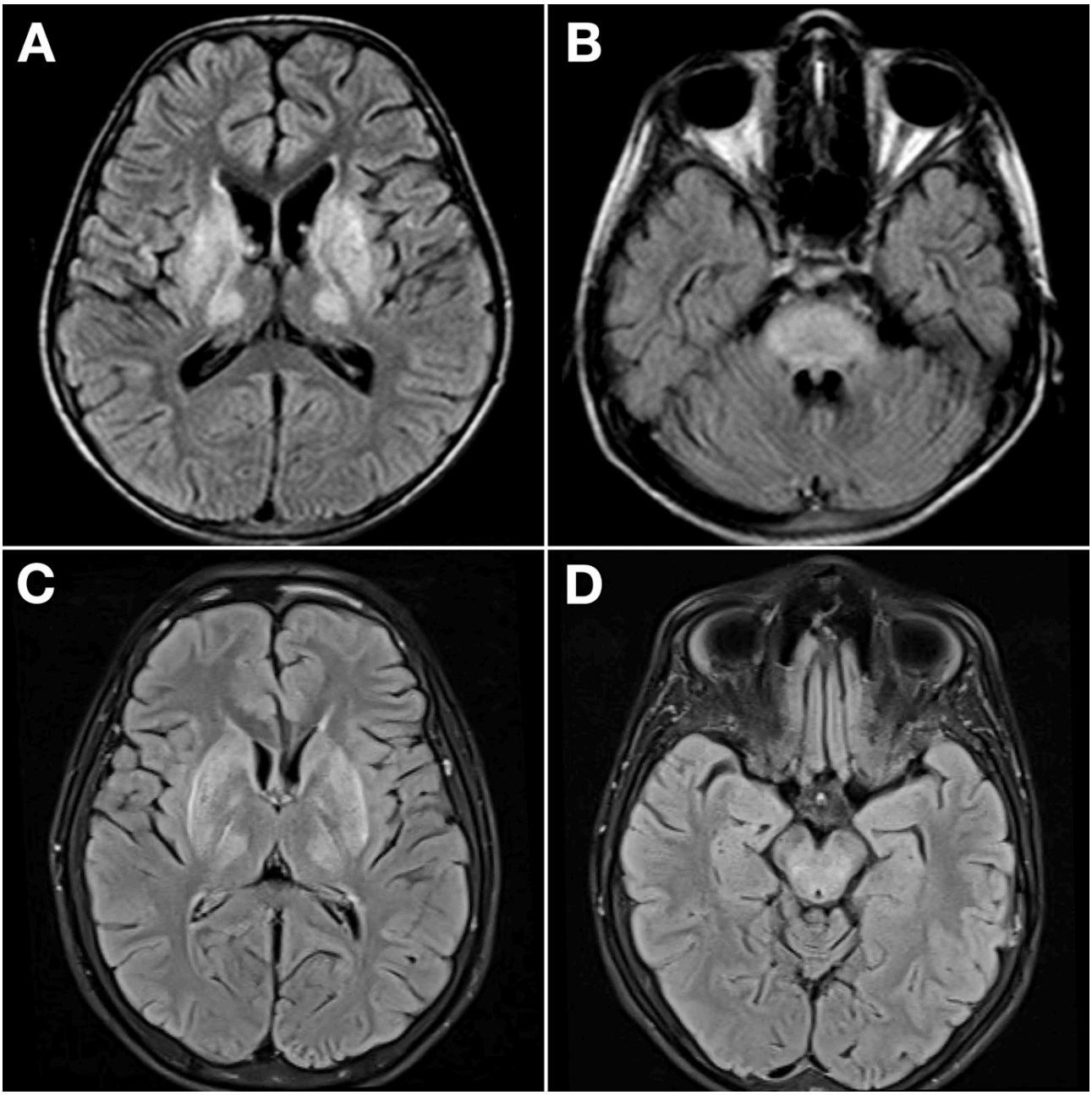


Figure 16. Wilson disease. **(A** and **B**) Bilateral FLAIR hyperintensity in the basal ganglia, anterolateral thalamus and pons. (**C** and **D**) Bilateral FLAIR signal in the basal ganglia, anterolateral thalamus and the midbrain in a separate case.

Images (A and B) courtesy of Paresh K Desai, Radiopaedia.org, rID 12107 (https://radiopaedia.org/cases/12107). Images (C and D) courtesy of Huda B Gharbia, Radiopaedia.org, rID 65738 (https://radiopaedia.org/cases/65738).

Key structural findings (MRI)	T2 finding are highly variable [68] [69]: • The most common abnormality is hyperintensity in the putamina. • Hyperintensity is relatively common in the caudate nuclei, globus pallidi, ventrolateral thalami and deep nuclei of the midbrain. • The cerebral hemispheres can be involved (~25%) creating a leukoencephalopathy appearance, with a frontal predominance. T1 findings are also variable, depending on the degree of oedema and hepatic dysfunction. The areas involved are similar to those described in the T2 findings. In patients presenting with neurological manifestations, T1 signal will be reduced. In patients presenting with hepatic dysfunction, T1 signal will be increased, especially in the globus pallidi. This is similar to the findings seen in acquired hepatocellular degeneration and is attributed to manganese deposition [68] [69]. Gradient echo sequence and susceptibility-weighted imaging: Occasionally, there can be blooming artefact in the areas described above, most commonly the putamen.
Nuclear medicine	Not routinely used.
Pitfalls	Imaging features are highly variable, making this a challenging diagnosis. Imaging features vary depending on whether the disease is treated or untreated and upon the degree of associated hepatic impairment.

Limbic Encephalitis/Autoimmune Encephalitis

Key structural findings (MRI)	Swelling and increased T2/FLAIR signal in the mesial temporal lobes and limbic system [70]. Bilateral involvement is most common (60%) [70] [71]. There may be more widespread involvement in the lateral temporal lobes, insula, basal ganglia and thalami. Diffusion restriction is unusual but may be present due to post-seizure changes. Enhancement and haemorrhage are rare.
Nuclear medicine	FDG PET: ↑ mesial temporal lobes [71]
Pitfalls	Findings may be very subtle. If there is uncertainty based on imaging appearances, short interval repeat MRI in the following weeks to months may be useful as the findings may become more apparent. Herpes simplex encephalitis can look similar but has a very different clinical context. A low-grade glioma can also look very similar and follow-up until resolution is therefore important. A large portion of cases are paraneoplastic and patients should be screened for an underlying malignancy if confirmed to have autoimmune encephalitis.

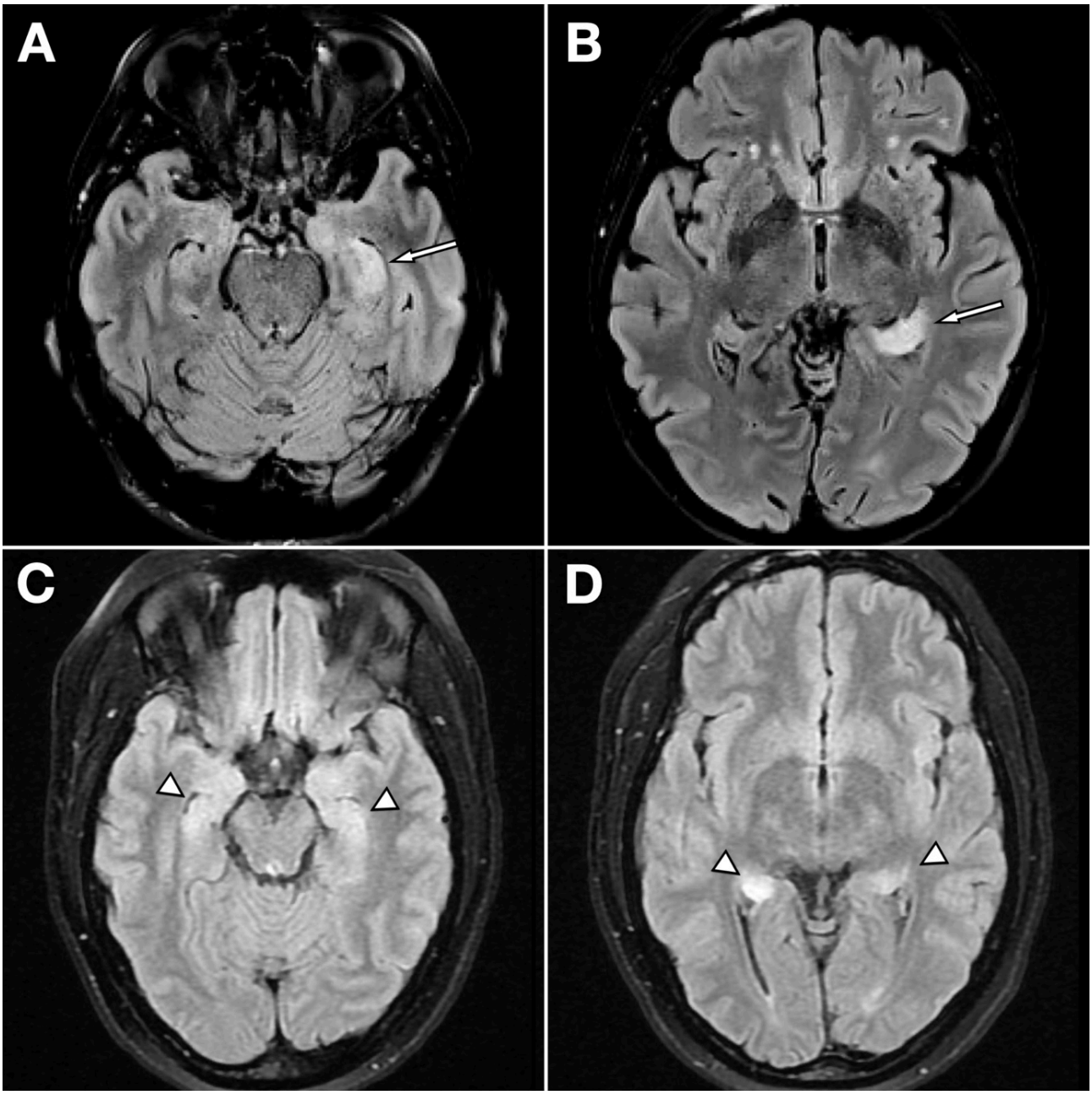


Figure 17. Limbic/autoimmune encephalitis. (**A** and **B**) Increased signal in the mesial left temporal lobe and throughout the left hippocampus in a case of anti-Hu antibody encephalitis. (**C** and **D**) Increased signal in the mesial temporal lobes and hippocampi bilaterally in a case of anti-NMDA antibody encephalitis.

Images (A and B) courtesy of Aurora Bolivar, Radiopaedia.org, rID 96138 (https://radiopaedia.org/cases/96138). Images (C and D) courtesy of Ashesh Ishwarlal Ranchod, Radiopaedia.org rID 170669 (https://radiopaedia.org/cases/170669).

Normal Pressure Hydrocephalus

Key structural findings (MRI)	Enlarged ventricles (elevated Evans index) [72] [73] Acute callosal angle (compared to normal controls and patients with AD) [74] Disproportionately enlarged subarachnoid space hydrocephalus (DESH): sylvian fissure enlargement, vertex crowding
Supportive findings	Increased aqueductal CSF flow rate and stroke volume [75]

Nuclear medicine	$^{111}In/^{99m}Tc$DTPA cisternography: abnormal radiotracer reflux into ventricles, persistent intraventricular activity, delayed migration to convexities [76]
Pitfalls	True hydrocephalus vs atrophy Excluding other causes for hydrocephalus

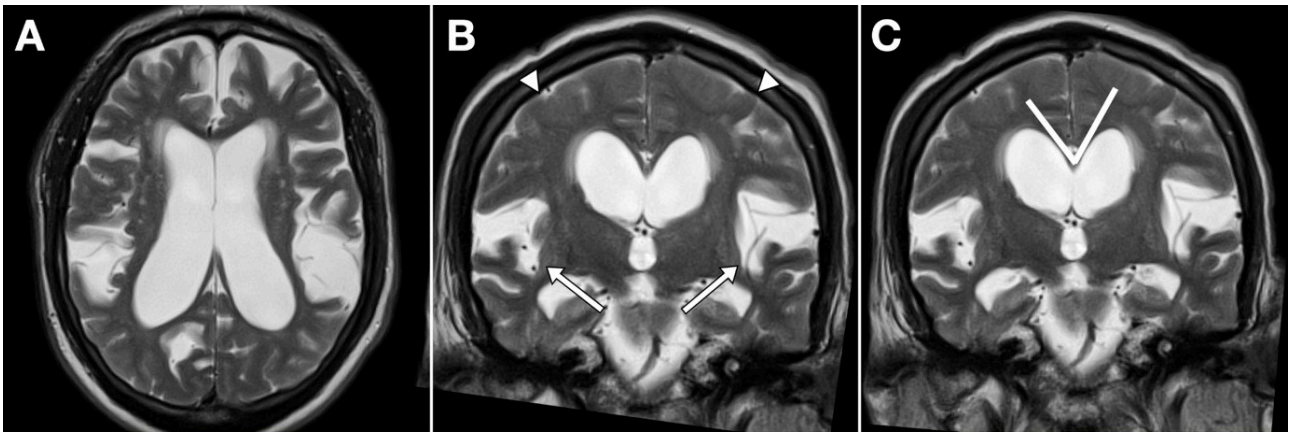


Figure 18. Normal pressure hydrocephalus. (**A**) Hydrocephalus and (**B**) disproportionate enlargement of the subarachnoid spaces in the sylvian fissure (white arrows) relative to the vertex (white arrow heads) and (**C**) acute callosal angle (53º, normal is >90º).

Case courtesy of Mostafa Elfeky, Radiopaedia.org, rID 73685 (https://radiopaedia.org/cases/73685).

NPH is a difficult clinical and radiological diagnosis. On structural imaging, the lateral and third cerebral ventricles are enlarged, with disproportionate widening of the sylvian fissures and gyral crowding at the vertex ('disproportionately enlarged subarachnoid space hydrocephalus', or DESH) [72]. Quantitative measures such as callosal angle are supportive, but not diagnostic in isolation and prone to error if not measured appropriately (for example, the callosal angle should be measured on coronal imaging, orthogonal to the anterior-posterior commissure plane at the level of the posterior commissure). Quantitative morphometry-based assessments may have higher diagnostic accuracy [77]. CSF flow through the cerebral aqueduct can be quantified on phase-contrast MRI sequences and in an early study predicted clinical response to shunting [78], although subsequently this has been found inconsistently [79] and there is currently no general consensus on reliable imaging predictors of response to shunting [80].

Creutzfeldt-Jakob disease

Key structural findings (MRI)	Findings can affect the cerebral cortex, most commonly the insula, cingulate gyrus and superior frontal gyrus, and the deep grey matter, most commonly the caudate nucleus and putamen but can also affect the thalamus [81 82]. Diffusion-weighted imaging: The most sensitive sequence with more pronounced findings than T2 and FLAIR due to a combination of true diffusion restriction and T2 shine through [81 82]. • Cortical ribboning: Gyriform diffusion restriction, a non-specific sign. • Pulvinar sign: High signal in the pulvinar nucleus of the thalamus. • Hockey stick sign: A combination of the pulvinar sign with high signal in the medial thalamus creating a hockey stick appearance of signal abnormality. A similar appearance can be seen in Wernicke encephalopathy. ADC: Variable depending on the timing of imaging from the onset of symptoms [81 82]. • Early: Low values, may be seen before DWI and FLAIR changes. • Late: Pseudonormalise or facilitated diffusion (high values), associated with atrophy. T2/FLAIR: Subtle hyperintensity, which may be absent early in the disease [82].
Nuclear medicine	Not routinely used.
Pitfalls	It is important to only suggest CJD in the appropriate clinical setting. Once the possibility of CJD is raised, obtaining tissue diagnosis can be difficult. Any instruments used need to be disposed of or quarantined until a diagnosis is established as there are cases of iatrogenic transmission of CJD via medical instruments.

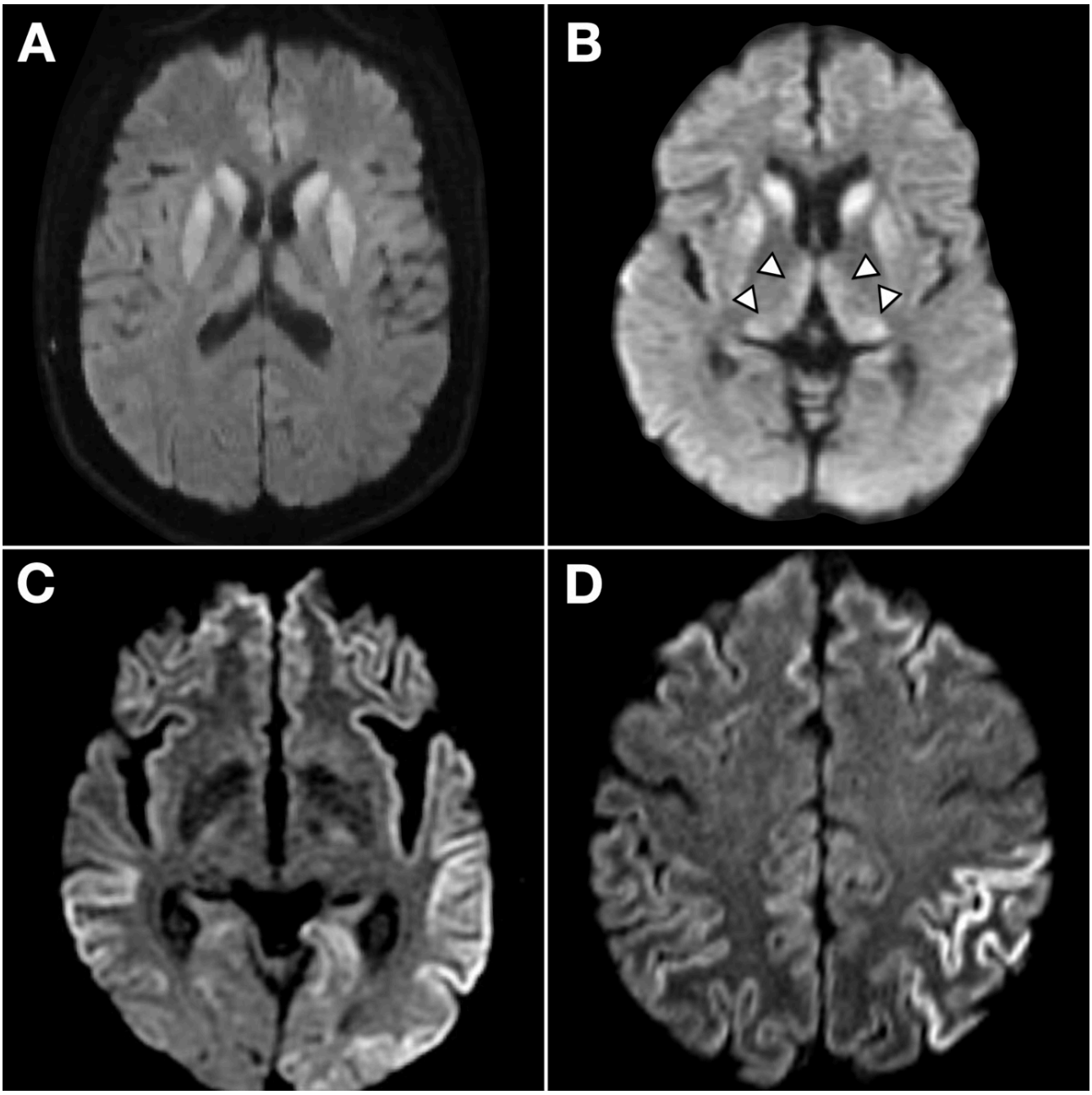


Figure 19. Creutzfeldt-Jakob disease. (**A** and **B**) Increased signal in the basal ganglia bilaterally and (**B**) increased signal in the medial and posterior thalami (hockey stick sign). (**C** and **D**) Multifocal increased cortical signal on DWI (cortical ribboning).

Image (A) courtesy of Brad Hayhow, Radiopaedia.org, rID 43970 (https://radiopaedia.org/cases/43970). Image (B) courtesy of Maxime St-Amant, Radiopaedia.org, rID 18712 (https://radiopaedia.org/cases/18712). Image (C) courtesy of Mathieu Deltomme, Radiopaedia.org, rID 54199 (https://radiopaedia.org/cases/54199). Image (D) courtesy of Chris O'Connell, Radiopaedia.org, rID 16320 (https://radiopaedia.org/cases/16320).

HIV-Associated Dementia (HIV Encephalopathy)

Key structural findings (MRI)	Diffuse and symmetric age-inappropriate cerebral atrophy [83]. Symmetrical periventricular white matter hyperintensity on T2/FLAIR with relative subcortical sparing. The posterior fossa is usually preserved.
Nuclear medicine	Not routinely used

HIV-associated neurocognitive disorders (HAND) is a group of clinical syndromes associated with HIV infection [84]. The group includes, in order of mild to severe, asymptomatic neurocognitive impairment, mild neurocognitive disorder and HIV-associated dementia, with the latter stages demonstrating progressive periventricular white matter signal changes and subcortical atrophy [85].

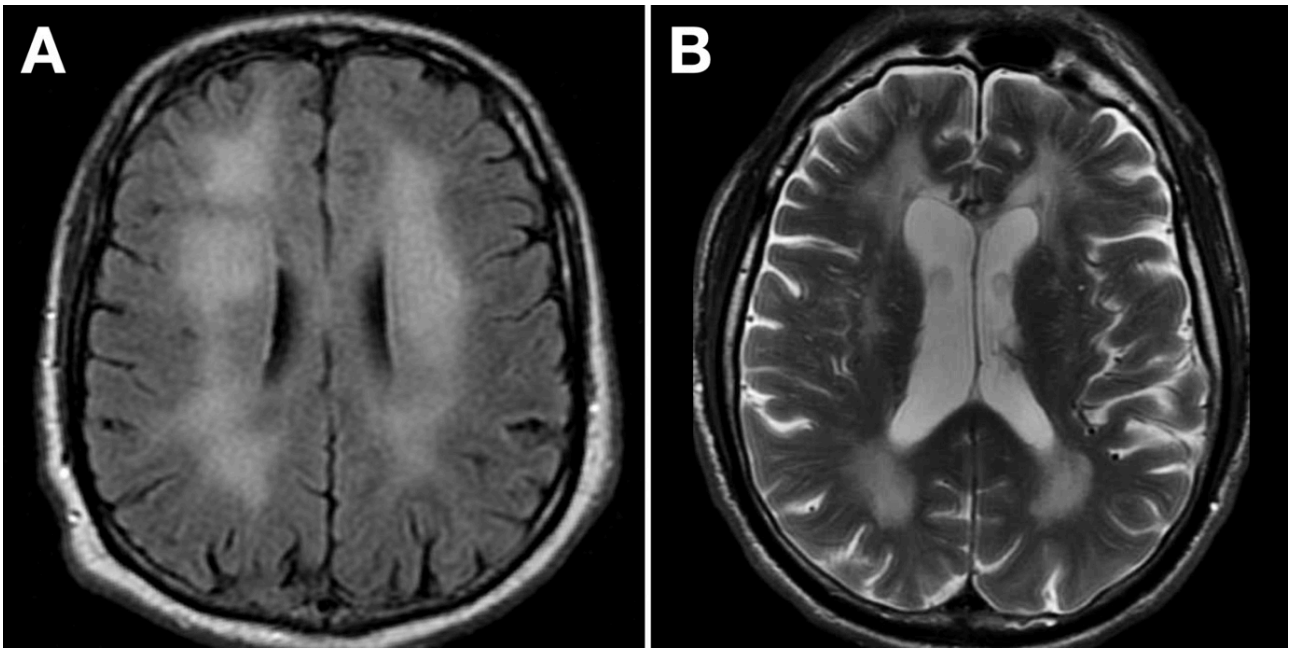


Figure 20. (**A** and **B**) Symmetric periventricular FLAIR and T2 white matter hyperintensity with subcortical sparing in two separate cases.

Image (A) courtesy of Frank Gaillard, Radiopaedia.org, rID 73685 (https://radiopaedia.org/cases/73685). Image (B) courtesy of Roberto Schubert, Radiopaedia.org, rID 14095 (https://radiopaedia.org/cases/14095).

References

1 Patel, K. P., Wymer, D. T., Bhatia, V. K., Duara, R. & Rajadhyaksha, C. D. Multimodality Imaging of Dementia: Clinical Importance and Role of Integrated Anatomic and Molecular Imaging. *Radiographics* **40**, 200-222 (2020). https://doi.org/10.1148/rg.2020190070

2 Patel, D. D., Leslie, S. W. & Shetty, M. in *StatPearls* (StatPearls Publishing

Copyright © 2026, StatPearls Publishing LLC., 2026).

3 Morris, E. *et al.* Diagnostic accuracy of 18F amyloid PET tracers for the diagnosis of Alzheimer's disease: a systematic review and meta-analysis. *European Journal of Nuclear Medicine and Molecular Imaging* **43**, 374-385 (2016). https://doi.org/10.1007/s00259-015-3228-x

4 Ashburner, J. & Friston, K. J. Voxel-based morphometry--the methods. *Neuroimage* **11**, 805-821 (2000). https://doi.org/10.1006/nimg.2000.0582

5 Bakshi, R., Ariyaratana, S., Benedict, R. H. B. & Jacobs, L. Fluid-Attenuated Inversion Recovery Magnetic Resonance Imaging Detects Cortical and Juxtacortical Multiple Sclerosis Lesions. *Archives of Neurology* **58**, 742-748 (2001). https://doi.org/10.1001/archneur.58.5.742

6 Wu, Z. *et al.* Identification of calcification with MRI using susceptibility-weighted imaging: a case study. *J Magn Reson Imaging* **29**, 177-182 (2009). https://doi.org/10.1002/jmri.21617

7 Hagmann, P. *et al.* Understanding diffusion MR imaging techniques: from scalar diffusion-weighted imaging to diffusion tensor imaging and beyond. *Radiographics* **26 Suppl 1**, S205-223 (2006). https://doi.org/10.1148/rg.26si065510

8 Minoshima, S., Cross, D., Thientunyakit, T., Foster, N. L. & Drzezga, A. ¹⁸F-FDG PET Imaging in Neurodegenerative Dementing Disorders: Insights into Subtype Classification, Emerging Disease Categories, and Mixed Dementia with Copathologies. *Journal of Nuclear Medicine* **63**, 2S-12S (2022). https://doi.org/10.2967/jnumed.121.263194

9 Chapleau, M., Iaccarino, L., Soleimani-Meigooni, D. & Rabinovici, G. D. The Role of Amyloid PET in Imaging Neurodegenerative Disorders: A Review. *J Nucl Med* **63**, 13s-19s (2022). https://doi.org/10.2967/jnumed.121.263195

10 Rabinovici, G. D. *et al.* Updated Appropriate Use Criteria for Amyloid and Tau PET: A Report from the Alzheimer's Association and Society for Nuclear Medicine and Molecular Imaging Workgroup. *Journal of Nuclear Medicine* **66**, S5-S31 (2025). https://doi.org/10.2967/jnumed.124.268756

11 Groot, C., Villeneuve, S., Smith, R., Hansson, O. & Ossenkoppele, R. Tau PET Imaging in Neurodegenerative Disorders. *Journal of Nuclear Medicine* **63**, 20S-26S (2022). https://doi.org/10.2967/jnumed.121.263196

12 Stormezand, G. N., Doorduin, J., Glaudemans, A., van der Hoorn, A. & De Jong, B. M. Current Developments on [(18)F]FDG PET/CT in Inflammatory Disorders of the Central Nervous System. *Semin Nucl Med* **55**, 503-511 (2025). https://doi.org/10.1053/j.semnuclmed.2025.06.001

13 Orunmuyi, A. T. *et al.* Structured reading for Tau PET Imaging in Alzheimer's disease and related dementias. *Seminars in Nuclear Medicine* (2026). https://doi.org/https://doi.org/10.1053/j.semnuclmed.2026.02.005

14 Jones, D., Pelak, V. & Rogalski, E. Atypical Presentations of Alzheimer Disease. *Continuum (Minneap Minn)* **30**, 1614-1641 (2024). https://doi.org/10.1212/con.0000000000001504

15 Raket, L. L. *et al.* Estimating the time course of biomarker changes in Alzheimer's disease. *Brain* (2025). https://doi.org/10.1093/brain/awaf413

16 Li, Y. *et al.* Timing of Biomarker Changes in Sporadic Alzheimer's Disease in Estimated Years from Symptom Onset. *Ann Neurol* **95**, 951-965 (2024). https://doi.org/10.1002/ana.26891

17 Lu, M. *et al.* Posttreatment Amyloid Levels and Clinical Outcomes Following Donanemab for Early Symptomatic Alzheimer Disease: A Secondary Analysis of the TRAILBLAZER-ALZ 2 Randomized Clinical Trial. *JAMA Neurol* **82**, 1251-1256 (2025). https://doi.org/10.1001/jamaneurol.2025.3869

18 Firth, N. C. *et al.* Longitudinal neuroanatomical and cognitive progression of posterior cortical atrophy. *Brain* **142**, 2082-2095 (2019). https://doi.org/10.1093/brain/awz136

19 Aziz, A. L. *et al.* Difference in imaging biomarkers of neurodegeneration between early and late-onset amnestic Alzheimer's disease. *Neurobiol Aging* **54**, 22-30 (2017). https://doi.org/10.1016/j.neurobiolaging.2017.02.010

20 Cash, D. M. *et al.* The pattern of atrophy in familial Alzheimer disease: volumetric MRI results from the DIAN study. *Neurology* **81**, 1425-1433 (2013). https://doi.org/10.1212/WNL.0b013e3182a841c6

21 Nelson, P. T. *et al.* Limbic-predominant age-related TDP-43 encephalopathy (LATE): consensus working group report. *Brain* **142**, 1503-1527 (2019). https://doi.org/10.1093/brain/awz099

22 Jäkel, L., De Kort, A. M., Klijn, C. J. M., Schreuder, F. & Verbeek, M. M. Prevalence of cerebral amyloid angiopathy: A systematic review and meta-analysis. *Alzheimers Dement* **18**, 10-28 (2022). https://doi.org/10.1002/alz.12366

23 Charidimou, A. *et al.* Emerging concepts in sporadic cerebral amyloid angiopathy. *Brain* **140**, 1829-1850 (2017). https://doi.org/10.1093/brain/awx047

24 van Dyck, C. H. *et al.* Lecanemab in Early Alzheimer's Disease. *N Engl J Med* **388**, 9-21 (2023). https://doi.org/10.1056/NEJMoa2212948

25 Sims, J. R. *et al.* Donanemab in Early Symptomatic Alzheimer Disease: The TRAILBLAZER-ALZ 2 Randomized Clinical Trial. *Jama* **330**, 512-527 (2023). https://doi.org/10.1001/jama.2023.13239

26 Fox, N. C. *et al.* Treatment for Alzheimer's disease. *Lancet* **406**, 1408-1423 (2025). https://doi.org/10.1016/s0140-6736(25)01329-7

27 Révész, T., Hawkins, C. P., du Boulay, E. P., Barnard, R. O. & McDonald, W. I. Pathological findings correlated with magnetic resonance imaging in subcortical arteriosclerotic encephalopathy (Binswanger's disease). *Journal of Neurology, Neurosurgery & Psychiatry* **52**, 1337-1344 (1989). https://doi.org/10.1136/jnnp.52.12.1337

28 Pascual, B. *et al.* Brain Glucose Metabolism in Vascular White Matter Disease With Dementia Differentiation From Alzheimer Disease. *Stroke; a journal of cerebral circulation* **41**, 2889-2893 (2010). https://doi.org/10.1161/STROKEAHA.110.591552

29 O'Brien, J. T. & Thomas, A. Vascular dementia. *Lancet* **386**, 1698-1706 (2015). https://doi.org/10.1016/s0140-6736(15)00463-8

30 Park, J.-H. *et al.* Pathogenesis of cerebral microbleeds: In vivo imaging of amyloid and subcortical ischemic small vessel disease in 226 individuals with cognitive impairment. *Annals of Neurology* **73**, 584-593 (2013). https://doi.org/https://doi.org/10.1002/ana.23845

31 Sachdev, P. S. *et al.* Vascular Cognitive Impairment and Dementia: Clinical Features, Neuropathology, and Biomarkers. *J Am Coll Cardiol* **87**, 52-76 (2026). https://doi.org/10.1016/j.jacc.2025.11.008

32 Planche, V. *et al.* Anatomical MRI staging of frontotemporal dementia variants. *Alzheimers Dement* **19**, 3283-3294 (2023). https://doi.org/10.1002/alz.12975

33 Shams, S. *et al.* MRI of the Swallow Tail Sign: A Useful Marker in the Diagnosis of Lewy Body Dementia? *American Journal of Neuroradiology* **38**, 1737-1741 (2017). https://doi.org/10.3174/ajnr.A5274

34 Kornienko, V. N. & Pronin, I. N. *Diagnostic Neuroradiology*. (Springer Berlin Heidelberg, 2008).

35 Whitwell, J. L. *et al.* Focal atrophy in dementia with Lewy bodies on MRI: a distinct pattern from Alzheimer's disease. *Brain* **130**, 708-719 (2007). https://doi.org/10.1093/brain/awl388

36 Fu, Y. & Halliday, G. M. Dementia with Lewy bodies and Parkinson disease dementia — the same or different and is it important? *Nature Reviews Neurology* **21**, 394-403 (2025). https://doi.org/10.1038/s41582-025-01090-x

37 McKeith, I. *et al.* Sensitivity and specificity of dopamine transporter imaging with ¹²³I-FP-CIT SPECT in dementia with Lewy bodies: a phase III, multicentre study. *The Lancet Neurology* **6**, 305-313 (2007). https://doi.org/10.1016/S1474-4422(07)70057-1

38 Mollenhauer, B. *et al.* Lewy Body and Parkinsonian Dementia. *Dtsch Arztebl International* **107**, 684-691 (2010).

39 Lim, S. M. *et al.* The ¹⁸F-FDG PET Cingulate Island Sign and Comparison to ¹²³I-β-CIT SPECT for Diagnosis of Dementia with Lewy Bodies. *Journal of Nuclear Medicine* **50**, 1638 (2009). https://doi.org/10.2967/jnumed.109.065870

40 Brown, R. K. J., Bohnen, N. I., Wong, K. K., Minoshima, S. & Frey, K. A. Brain PET in Suspected Dementia: Patterns of Altered FDG Metabolism. *RadioGraphics* **34**, 684-701 (2014). https://doi.org/10.1148/rg.343135065

41 Diaz-Galvan, P. *et al.* β-Amyloid Load on PET Along the Continuum of Dementia With Lewy Bodies. *Neurology* **101**, e178-e188 (2023). https://doi.org/10.1212/WNL.0000000000207393

42 Cummings, J. L. *et al.* The role of dopaminergic imaging in patients with symptoms of dopaminergic system neurodegeneration. *Brain* **134**, 3146-3166 (2011). https://doi.org/10.1093/brain/awr177

43 Nerattini, M., Abenavoli, E. M. & Berti, V. PET/CT in Movement Disorders: Update. *Semin Nucl Med* **55**, 565-576 (2025). https://doi.org/10.1053/j.semnuclmed.2025.03.007

44 Schwarz, S. T. *et al.* The 'swallow tail' appearance of the healthy nigrosome - a new accurate test of Parkinson's disease: a case-control and retrospective cross-sectional MRI study at 3T. *PLoS One* **9**, e93814 (2014). https://doi.org/10.1371/journal.pone.0093814

45 Kim, D., Tung, G., Akbar, U. & Friedman, J. The evaluation of the swallow tail sign in patients with parkinsonism and gait disorders. *Journal of the Neurological Sciences* **428**, 117581 (2021). https://doi.org/10.1016/j.jns.2021.117581

46 Wenning, G. K. *et al.* The Movement Disorder Society Criteria for the Diagnosis of Multiple System Atrophy. *Movement Disorders* **37**, 1131-1148 (2022). https://doi.org/https://doi.org/10.1002/mds.29005

47 Lee, W. H., Lee, C. C., Shyu, W. C., Chong, P. N. & Lin, S. Z. Hyperintense putaminal rim sign is not a hallmark of multiple system atrophy at 3T. *AJNR Am J Neuroradiol* **26**, 2238-2242 (2005).

48 Picillo, M. *et al.* Midbrain MRI assessments in progressive supranuclear palsy subtypes. *Journal of Neurology, Neurosurgery & Psychiatry* **91**, 98 (2020). https://doi.org/10.1136/jnnp-2019-321354

49 Oba, H. *et al.* New and reliable MRI diagnosis for progressive supranuclear palsy. *Neurology* **64**, 2050-2055 (2005). https://doi.org/10.1212/01.WNL.0000165960.04422.D0

50 Gröschel, K., Kastrup, A., Litvan, I. & Schulz, J. B. Penguins and hummingbirds: Midbrain atrophy in progressive supranuclear palsy. *Neurology* **66**, 949-950 (2006). https://doi.org/10.1212/01.wnl.0000203342.77115.bf

51 Righini, A. *et al.* MR imaging of the superior profile of the midbrain: differential diagnosis between progressive supranuclear palsy and Parkinson disease. *AJNR Am J Neuroradiol* **25**, 927-932 (2004).

52 Tokumaru, A. M. *et al.* Corticobasal degeneration: MR with histopathologic comparison. *AJNR Am J Neuroradiol* **17**, 1849-1852 (1996).

53 Armstrong, M. J. *et al.* Criteria for the diagnosis of corticobasal degeneration. *Neurology* **80**, 496-503 (2013). https://doi.org/10.1212/WNL.0b013e31827f0fd1

54 Lövblad, K. O. *et al.* MR Imaging in Multiple Sclerosis: Review and Recommendations for Current Practice. *American Journal of Neuroradiology* **31**, 983 (2010). https://doi.org/10.3174/ajnr.A1906

55 Lisanti, C. J., Asbach, P. & Bradley, W. G., Jr. The ependymal "Dot-Dash" sign: an MR imaging finding of early multiple sclerosis. *AJNR Am J Neuroradiol* **26**, 2033-2036 (2005).

56 Andravizou, A. *et al.* Brain atrophy in multiple sclerosis: mechanisms, clinical relevance and treatment options. *Autoimmunity Highlights* **10**, 7 (2019). https://doi.org/10.1186/s13317-019-0117-5

57 Ciccarelli, O. *et al.* Spinal cord involvement in multiple sclerosis and neuromyelitis optica spectrum disorders. *The Lancet Neurology* **18**, 185-197 (2019). https://doi.org/10.1016/S1474-4422(18)30460-5

58 Provenzale, J. M. Imaging of Traumatic Brain Injury: A Review of the Recent Medical Literature. *American Journal of Roentgenology* **194**, 16-19 (2010). https://doi.org/10.2214/AJR.09.3687

59 Lee, B. & Newberg, A. Neuroimaging in traumatic brain imaging. *NeuroRX* **2**, 372-383 (2005). https://doi.org/10.1602/neurorx.2.2.372

60 Orr, T. J. *et al.* Traumatic Brain Injury: A Comprehensive Review of Biomechanics and Molecular Pathophysiology. *World Neurosurg* **185**, 74-88 (2024). https://doi.org/10.1016/j.wneu.2024.01.084

61 Sharma, B., Monteiro, L., Changoor, A., Colella, B. & Green, R. The Scale of Neurodegeneration in Moderate-to-Severe Traumatic Brain Injury: A Systematic Review of Longitudinal Studies. *Ann Neurol* **98**, 668-681 (2025). https://doi.org/10.1002/ana.27279

62 Cheung, G. *et al.* Amyotrophic lateral sclerosis: correlation of clinical and MR imaging findings. *Radiology* **194**, 263-270 (1995). https://doi.org/10.1148/radiology.194.1.7997565

63 Chakraborty, S., Gupta, A., Nguyen, T. & Bourque, P. The “Motor Band Sign:” Susceptibility-Weighted Imaging in Amyotrophic Lateral Sclerosis. *Canadian Journal of Neurological Sciences / Journal Canadien des Sciences Neurologiques* **42**, 260-263 (2015). https://doi.org/10.1017/cjn.2015.40

64 Fox, M. D. & Cohen, A. B. “Bright tongue sign” in ALS. *Neurology* **79**, 1520-1520 (2012). https://doi.org/10.1212/WNL.0b013e31826d5ffc

65 Negi, R. S., Manchanda, K. L. & Sanga, S. Imaging of Huntington's disease. *Medical Journal Armed Forces India* **70**, 386-388 (2014). https://doi.org/https://doi.org/10.1016/j.mjafi.2012.08.002

66 Seddighi, S., Bang, J. & Deng, F. Fast-track to a Huntington disease diagnosis – I saw the “box-car” sign. *Clinical Imaging* **125** (2025). https://doi.org/10.1016/j.clinimag.2025.110568

67 Rosas, H. D. *et al.* Regional cortical thinning in preclinical Huntington disease and its relationship to cognition. *Neurology* **65**, 745-747 (2005). https://doi.org/10.1212/01.wnl.0000174432.87383.87

68 Patel, K., Bhayana, A., Bagri, N. & Malik, A. Case series on neuroimaging spectrum of Wilson’s disease: knowing the known and the uncommonly known. *Egyptian Journal of Radiology and Nuclear Medicine* **55** (2024). https://doi.org/10.1186/s43055-024-01328-6

69 Yu, X. E., Gao, S., Yang, R. M. & Han, Y. Z. MR Imaging of the Brain in Neurologic Wilson Disease. *American Journal of Neuroradiology* **40**, 178 (2019). https://doi.org/10.3174/ajnr.A5936

70 Sanvito, F. *et al.* Autoimmune encephalitis: what the radiologist needs to know. *Neuroradiology* **66**, 653-675 (2024). https://doi.org/10.1007/s00234-024-03318-x

71 Oyanguren, B. *et al.* Limbic encephalitis: a clinical-radiological comparison between herpetic and autoimmune etiologies. *European Journal of Neurology* **20**, 1566-1570 (2013). https://doi.org/https://doi.org/10.1111/ene.12249

72 Shinoda, N. *et al.* Utility of MRI-based disproportionately enlarged subarachnoid space hydrocephalus scoring for predicting prognosis after surgery for idiopathic normal pressure hydrocephalus: clinical research. *Journal of Neurosurgery* **127**, 1436-1442 (2017). https://doi.org/https://doi.org/10.3171/2016.9.JNS161080

73 Kockum, K. *et al.* The idiopathic normal-pressure hydrocephalus Radscale: a radiological scale for structured evaluation. *European Journal of Neurology* **25**, 569-576 (2018). https://doi.org/https://doi.org/10.1111/ene.13555

74 Ishii, K. *et al.* Clinical impact of the callosal angle in the diagnosis of idiopathic normal pressure hydrocephalus. *Eur Radiol* **18**, 2678-2683 (2008). https://doi.org/10.1007/s00330-008-1044-4

75 Hayhow, B., Begic, F., Evans, A., Velakoulis, D. & Gaillard, F. Communicating hydrocephalus with reversible cognitive impairment. *Australian & New Zealand Journal of Psychiatry* **48**, 379-380 (2014). https://doi.org/10.1177/0004867413511547

76 Thut, D. P., Kreychman, A. & Obando, J. A. ^{111}In-DTPA cisternography with SPECT/CT for the evaluation of normal pressure hydrocephalus. *J Nucl Med Technol* **42**, 70-74 (2014). https://doi.org/10.2967/jnmt.113.128041

77 Yun, S. Y. *et al.* Risk estimation for idiopathic normal-pressure hydrocephalus: development and validation of a brain morphometry-based nomogram. *Eur Radiol* **33**, 6145-6156 (2023). https://doi.org/10.1007/s00330-023-09612-1

78 Bradley, W. G., Jr. *et al.* Normal-pressure hydrocephalus: evaluation with cerebrospinal fluid flow measurements at MR imaging. *Radiology* **198**, 523-529 (1996). https://doi.org/10.1148/radiology.198.2.8596861

79 Whitley, H., Skalický, P., Zazay, A., Bubeníková, A. & Bradáč, O. Volumes and velocities: Meta-analysis of PC-MRI studies in normal pressure hydrocephalus. *Acta Neurochir (Wien)* **166**, 463 (2024). https://doi.org/10.1007/s00701-024-06333-2

80 Johnson, M. D. & Williams, M. A. Idiopathic Normal-Pressure Hydrocephalus. *N Engl J Med* **393**, 2243-2253 (2025). https://doi.org/10.1056/NEJMra2306506

81 Vitali, P. *et al.* Diffusion-weighted MRI hyperintensity patterns differentiate CJD from other rapid dementias. *Neurology* **76**, 1711-1719 (2011). https://doi.org/10.1212/WNL.0b013e31821a4439

82 Tschampa, H. J. *et al.* Pattern of Cortical Changes in Sporadic Creutzfeldt-Jakob Disease. *American Journal of Neuroradiology* **28**, 1114 (2007). https://doi.org/10.3174/ajnr.A0496

83 Sakai, M. *et al.* MRI imaging features of HIV-related central nervous system diseases: diagnosis by pattern recognition in daily practice. *Japanese Journal of Radiology* **39**, 1023-1038 (2021). https://doi.org/10.1007/s11604-021-01150-4

84 Antinori, A. *et al.* Updated research nosology for HIV-associated neurocognitive disorders. *Neurology* **69**, 1789-1799 (2007). https://doi.org/10.1212/01.WNL.0000287431.88658.8b

85 Cilliers, K. & Muller, C. J. F. Effect of human immunodeficiency virus on the brain: A review. *The Anatomical Record* **304**, 1389-1399 (2021). https://doi.org/https://doi.org/10.1002/ar.24573